DEPARTMENT OF PHYSICS
UNIVERSITY OF JYVÄSKYLÄ
RESEARCH REPORT No. 11/2008

FERMIONIC SUPERFLUIDITY IN OPTICAL LATTICES

BY

TIMO KOPONEN

Academic Dissertation
for the Degree of
Doctor of Philosophy

To be presented, by permission of the
Faculty of Mathematics and Science
of the University of Jyväskylä,
for public examination in Auditorium FYS-1 of the
University of Jyväskylä on December 12, 2008
at 12 o'clock noon.

Jyväskylä, Finland
December 2008

Preface

This thesis is a summary of the research I have carried out during the years 2004-2008. I am fortunate to have been supervised by Prof. Päivi Törmä, whose vision and relentlessness have had a great influence on my work. I appreciate the efforts of Dr. Jani-Petri Martikainen in educating me in the craft of theoretical physics. I also acknowledge Dr. Jami Kinnunen, Mr. Tomi Paananen, Dr. Lars Melwyn Jensen, Dr. Reza Bakhtiari, and Mr. Joni Pasanen for the fruitful collaboration that has led to the publications included in this thesis.

I thank all the present and former members of our research group, in particular Mr. Tommi Hakala, Mr. Miikka Heikkinen, Mr. Jussi Kajala, Dr. Francesco Massel, and Mr. Marcus Rinkiö. Most importantly, however, I want to mention Mr. Mikko Leskinen for many enlightening and inspiring discussions. I would like to acknowledge Prof. Matti Manninen, Docent Juha Merikoski, and Prof. Vesa Ruuskanen for teaching and guidance. Of my colleagues outside our group I want to thank Ms. Ulrika Jakobsson, Mr. Panu Koppinen, Mr. Pauli Peura, Mr. Tommi Ropponen, and Ms. Laura Tuomikoski.

I am grateful to Dr. Seija Sirkiä for her support and her wisdom in all our endeavours.

Mr. Jussi Hokkanen, Mr. Atte Kaasinen, and Ms. Anne Peuhkuri have been a great source of encouragement. The people from Laukaan Shukokai Karate deserve my gratitude, especially Mr. Jouni Hirvonen, Mrs. Eva-Kaisa Niemistö, Ms. Hanna Niemistö, Mr. Veli-Pekka Niemistö and Ms. Sanna Närä. The guidance of Mr. Yrjö Pursiainen and Mr. Esa Kaplas has been extremely valuable.

Finally I thank my parents for all their support.

Support from the National Graduate School in Materials Physics, The Finnish Cultural Foundation, and the foundations of Ellen and Artturi Nyyssönen and Emil Aaltonen, is gratefully acknowledged.

Espoo, November 2008

Timo Koponen

Abstract

Koponen, Timo, 1979–
Fermionic superfluidity in optical lattices
Jyväskylä: University of Jyväskylä, 2008
(Research report/Department of Physics, University of Jyväskylä,
ISSN 0075-465X; 11/2008)
ISBN 978-951-39-3403-3

This is a study of the theory of ultracold atomic Fermi gases, especially in optical lattices, i.e. periodic potentials created with laser light. Superfluidity is studied especially in the case of spin population imbalanced Fermi gases and phase diagrams are calculated from mean field theory. The Fulde-Ferrel-Larkin-Ovchinnikov (FFLO) phase is shown to occupy a larger region of the phase diagram than previously predicted for purely harmonically trapped systems. Methods for detecting the FFLO phase are suggested. As another topic, excitations in a superfluid Fermi gas, their signatures and use in sensor applications are studied.

The thesis is divided in chapters in the following way: Chapter 1 is an introduction to the research field of ultracold quantum gases, including references to some of the most important experiments done with the fermionic isotopes. Chapter 2 is an introduction to optical lattices and their major experimental characteristics. Chapter 3 deals with extensions of BCS-theory, mainly the FFLO and the detection of the phases predicted by the extensions. In chapter 4 I discuss excitations in BCS-like states and their applications in sensing electro-magnetic fields. Chapter 5 contains the conclusions.

Keywords fermi gases, superfluidity, optical lattices, BCS-theory, FFLO phase

List of publications

This thesis consists of the following publications.

I T. KOPONEN, J.-P. MARTIKAINEN, J. KINNUNEN, AND P. TÖRMÄ, *Sound velocity and dimensional crossover in a superfluid Fermi gas in an optical lattice*, Phys. Rev. A **73** 033620 (2006).

II T. KOPONEN, J. KINNUNEN, J.-P. MARTIKAINEN, L.M. JENSEN, AND P. TÖRMÄ, *Fermion pairing with spin-density imbalance in an optical lattice*, New J. Phys. **8** 179 (2006).

III T.K. KOPONEN, T. PAANANEN, J.-P. MARTIKAINEN, AND P. TÖRMÄ, *Finite temperature phase diagram of a polarized Fermi gas in an optical lattice*, Phys. Rev. Lett. **99**, 120403 (2007).

IV T.K. KOPONEN, T. PAANANEN, J.-P. MARTIKAINEN, M.R. BAKHTIARI, AND P. TÖRMÄ, *FFLO state in 1, 2, and 3 dimensional optical lattices combined with a non-uniform background potential*, New J. Phys. **10** 045014 (2008).

V T.K. KOPONEN, J. PASANEN, AND P. TÖRMÄ, *Fermi condensates for dynamic imaging of electro-magnetic fields*, submitted to Phys. Rev. Lett., arXiv:0809.2959 (2008).

The author has performed most of the analytical calculations for all the publications. The author has done all the numerical analysis for publications I - III and V and most of the analysis for publication IV. The author is the main writer of publications I,II, and IV and has participated in writing publications III and V.

Contents

Chapter 1

Ultracold atomic gases

1.1 On quantum statistics

In classical physics, even identical particles are distinguishable. This means that if there were two completely identical particles in a confined volume, such as a box, we could attach a virtual label to them at some point in time, and by following their trajectories we would always know which one is which. In thermal equilibrium, the energy distribution of a large number of such particles would follow the Maxwell-Boltzmann distribution. However, in quantum mechanics such a distinction is impossible. Even if we were to label two identical particles at a given instant in time, according to quantum mechanics we would not be able to distinguish between them at any other time, because the concept of trajectory does not exist in quantum mechanics. Thus, in the context of quantum mechanics, identical particles are indistinguishable. As a result, their energy distribution is not the Maxwell-Boltzmann type.

It has turned out that in the three-dimensional world, in terms of energy distributions, or *statistics*, there are two kinds of particles. This is more a postulate of many-body quantum mechanics than a consequence, but the following explanation may shed light on the concept: whereas a classical system is described fully by listing at any point in time the positions and momenta of all the particles in it, a quantum mechanical system is completely described by giving its wave function at any point in time. The wave function is a function of all the observable variables (called quantum numbers) of the system, whose value is a complex number. In a simplified system these variables are the positions of all the particles. The absolute value of the wave function squared gives the probability of finding the system in a given configuration. Because no probabilities can change as a result of swapping the positions of two completely identical particles, the wavefunction (usually denoted by Ψ) must have the following

property:

$$|\Psi(\mathbf{x}_1, \mathbf{x}_2)|^2 = |\Psi(\mathbf{x}_2, \mathbf{x}_1)|^2,$$

i.e. the probability of finding particle 1 in location x_1 and particle 2 in location x_2 must be the same as finding the particles in the opposite positions. In a three-dimensional system there are two ways in which this is possible, either $\Psi(x_1, x_2) = \Psi(x_2, x_1)$ or $\Psi(x_1, x_2) = -\Psi(x_2, x_1)$. As a convention, particles whose wavefunction obeys the former are called bosons and the latter fermions. Experiments have confirmed that all the known particles (such as quarks, electrons, or protons) belong to either one of these groups. Related to this property of the wavefunction, these two types of particles have their own energy distributions, known as the Bose-Einstein distribution for bosons and Fermi-Dirac distribution for fermions.

The antisymmetry of the wavefunction gives a very distinct characteristic for fermions: as $\Psi(x_1, x_2) = -\Psi(x_2, x_1)$ it follows that $\Psi(x_1, x_1) = -\Psi(x_1, x_1)$, which means that $\Psi(x_1, x_1) = 0$ for identical fermions. This is a mathematical way of saying that the probability of finding two identical fermions in the same quantum state is zero, which is a fundamental property of many-body quantum mechanics, known as the *Pauli exclusion principle*. The exclusion principle is a very black-and-white kind of effect; the particles simply can not occupy the same state. In some sense this principle divides particles in two classes that are fermions and non-fermions, i.e. particles that obey the Pauli principle and the ones that do not.

For composite particles, i.e. particles composed of a bound state of two or more particles, the statistics is inherited in the following way: a composite of an odd number of fermions is a fermion, a composite of an even number of fermions is a boson. A composite of any number of bosons is a boson. Since quarks are fermions, protons and neutrons, being composed of three quarks, are fermions. As electrons are also fermions, the number of fermions in a neutral atom is $2Z+N$, Z being the number of protons and N the number of neutrons. Therefore the number of neutrons alone determines the type the atom is. So, even though the electron cloud determines all the chemical properties of the atom, the collective behaviour of a cold dilute gas of one isotope is determined by the neutrons in the nucleus.

Originally the study of ultracold atomic gases can be traced back to Satyendra Nath Bose who, together with Albert Einstein, put forward the theory of Bose-Einstein condensation in the 1920s [1, 2]. An essential feature of their prediction is that a cloud of bosonic particles would, if cooled down below a critical temperature, condense as what is nowadays known as a Bose-Einstein condensate (BEC). In this state, there is a macroscopic population of particles

in a single quantum state, thereby creating a kind of coherent matter wave. Although this state was observed with superfluid liquid helium, the strong interactions present in the system prevent the observation of a pure BEC, and therefore a condensate of non-interacting particles lacked satisfactory experimental proof until 1995, when the research groups of Carl Wieman and Eric Cornell at Boulder and Wolfgang Ketterle at MIT managed to cool clouds of rubidium (Wieman-Cornell) and sodium (Ketterle) atoms below their critical temperatures and observe their condensation [3, 4]. Since then, atomic BECs have been created and observed in numerous laboratories all around the world.

1.2 Cooling and trapping

Alkali atoms, that is atoms with just one electron occupying the outermost shell, are the ones commonly used for atom gas experiments. These elements are, in the order of increasing mass, hydrogen, lithium, sodium, potassium, rubidium, and cesium. In the ground state the inner shells are closed and thus they have no net angular momentum, and the outermost electron is in an s-orbit, also with no angular momentum. The outermost electron is the reason to the common use of alkali atoms in the experiments; because of the singly occupied shell, the atoms have suitable transitions with optical wavelengths, that can be utilized for cooling. A typical trapping scheme utilizes the hyperfine interaction, which is the coupling between the electronic spin and the spin of the nucleus and the dependence of the energies of the hyperfine states on the external magnetic field, called the Zeeman effect. The hyperfine states are characterized by their total spin F, which can have the values $I \pm 1/2$, where I is the nuclear spin, and their hyperfine magnetic moment m_F, ranging from $-F$ to F. In the absence of an external magnetic field, there is an energy difference between states $F = I - 1/2$ and $F = I + 1/2$, called hyperfine splitting, but the states with same F are degenerate. As the magnetic field couples to both the nuclear and electron spin, the states with different m_F become non-degenerate and split into levels called *Zeeman sublevels*. The corresponding energy splitting is called Zeeman splitting. It is important that the energy for some hyperfine states increases with the increasing magnetic field while for others it decreases. The former are called low field seeking and the latter high field seeking states, see figure 1.1. For weak magnetic fields the energy of all hyperfine states is linear as a function of the field strength.

Magnetic trapping of neutral atoms relies on the application of the Zeeman effect to trap atoms prepared in a low-field-seeking hyperfine state. In a magneto-optical trap (MOT) two magnetic coils in an anti-Helmholtz configuration are

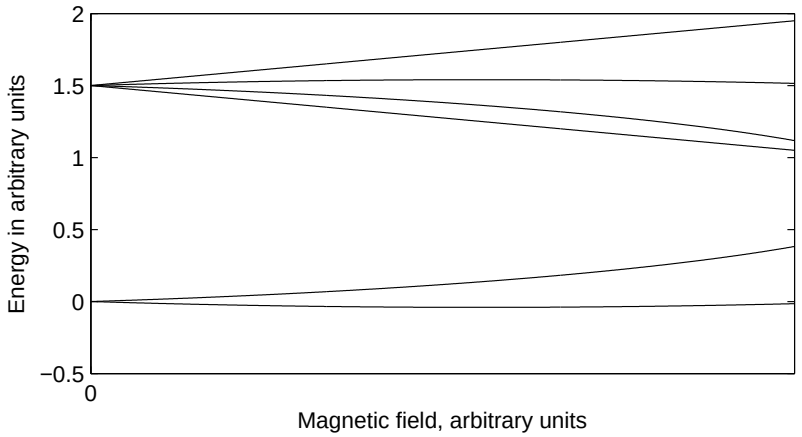

FIGURE 1.1: Schematic picture of the Zeeman effect for nuclear spin $I = 1$. The hyperfine manifold with $F = 1/2$ has two states and the one with $F = 3/2$ four. In a weak magnetic field the Zeeman splitting is much less than the hyperfine splitting, i.e. the energy difference of the hyperfine manifolds. Hyperfine states for which the energy increases as a function of magnetic field are low field seekers and those with decreasing energy high field seekers.

used to create a magnetic field with an amplitude minimum in the center of the system. The problem with such a setup is that the field actually vanishes in the center, allowing atoms to lose their orientation and flip to other hyperfine states, consequentially letting them escape the trap. In the original BEC experiments this was overcome by rotating the trap, thereby creating a pseudopotential with a maximum in the center (Boulder) or by "plugging" the hole in the center by a laser beam (MIT). Another way of trapping atoms magnetically is the Ioffe-Pritchard trap, which consists of two parallel coils with currents flowing in the same direction and four bars, known as Ioffe bars, carrying current parallel to the axis of the coils.

Atoms can also be trapped in optical traps operating on the principle of atom polarizability and its interaction with the electric field. As explained in more detail in the chapter on optical lattices, depending on the detuning of the laser, atoms are attracted to the locations of lowest or highest intensity of the electric field and can therefore be trapped in the middle of intersecting laser beams. All-optical trapping is experimentally convenient because there are no magnetic fields interfering with the so called Feshbach fields, explained below.

Atoms trapped in a MOT are cooled by laser cooling, which can be explained by the following picture: assume two laser beams, one propagating to the right and the other to the left, and assume there is an atom moving to the right in the field created by the lasers. The frequency of the lasers is tuned just below

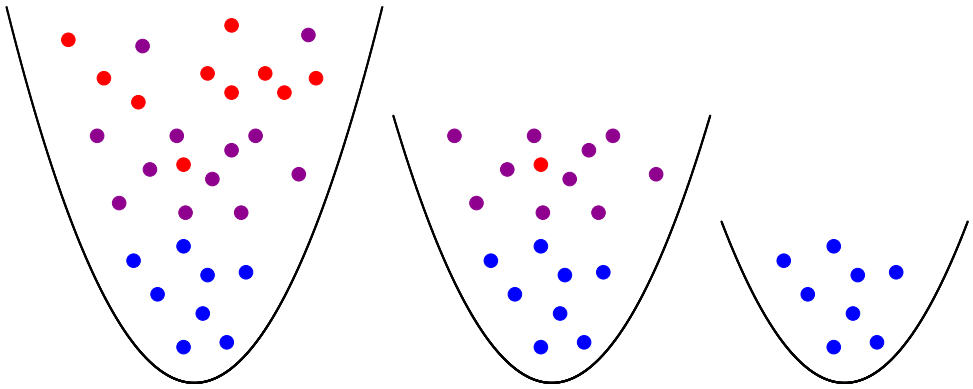

FIGURE 1.2: Successive cooling cycles in evaporative cooling. The height of the trapping potential is lowered and the gas is allowed to thermalize.

a transition between the ground and an excited state of the atom. Because of the Doppler effect, the atom experiences the frequency of the left moving photons as higher than that of the right moving ones, and the absorption rate of the former is higher than that of the latter. Though the atom decays back to the ground state by spontaneous emission, in this process the photon has a higher energy (the energy of the transition) than the initial absorbed photon. The energy difference is given by a loss in kinetic energy of the atom, leading to cooling. In a MOT, cooling is realized by three pairs of laser beams in perpendicular directions. The minimum temperature reachable by this method is of the order 100 µK, not low enough for realizing a BEC. This can be improved by using a so called Sisyphus cycle to achieve temperatures of the order 1 µK [5].

In order to cool the sample even more, a process called evaporative cooling is used. As a simplified picture, this can be understood as lowering the "edge" of the trapping potential, causing the atoms with the most kinetic energy, i.e. the hottest atoms, to escape and letting the gas thermalize. Repeating this process allows the cooling of the sample to very low temperatures, even as low as 10 nK. Because evaporative cooling works by deliberately letting some atoms escape the trap, it causes significant atom losses during the process; 90 % of the initial sample might be lost in the cooling. Therefore the largest possible number of atoms in the beginning of the process is desirable.

1.3 Atom-atom interactions

An essential feature of ultracold atom gases is their diluteness: with densities below 10^{20} m^{-3}, the interparticle distance is larger than 100 nm, 100 to 1000

times longer than in a solid. This extreme diluteness means that two-body collisions are the dominant form of interaction and processes involving three or more atoms can be neglected. Thus the physics involved can mostly be derived from the two-body scattering theory.

The real interaction potential between two atoms is a van der Waals type potential, with hard core repulsion at distances $r \leqslant r_c$ and attraction proportional to r^{-6} with $r >> r_c$, shown in figure 1.3. This potential has a number of bound states. However, the use of this potential is not practical in calculations because of its complicated form. Because we are interested in many-body phenomena in low temperatures, i.e. with low scattering energies, we can afford to approximate the potential with an effective pseudopotential of the form given by

$$V(\mathbf{r})\psi(\mathbf{r}) = g\delta(\mathbf{r}) \left[\frac{\partial}{\partial r}(r\psi(\mathbf{r}))\right]_{r=0}, \tag{1.1}$$

with $g = 4\pi\hbar^2 a/m$, where a is called the s-wave scattering length and m is the mass of the atom. All features of the low-energy scattering of two particles, such as atoms, are described by the single parameter a. The intriguing feature of the scattering process is that a can be controlled with an external magnetic field, using a phenomenon known as the Feshbach resonance [6, 7, 8]. In the scattering process a molecular state can couple resonantly to the free state through a virtual process. Depending on the energy difference of the free state and the molecular state, which can be controlled by the magnetic field, the scattering length can have any value. The s-wave scattering length, as a function of the magnetic field, is shown schematically in figure 1.4.

The Feshbach resonance offers an invaluable tool for choosing the strength of the effective interaction and even whether it is attractive or repulsive, by applying a magnetic field. This is one of the key features in making ultracold atom gases a suitable "test bench" for ideas and models concerning many-body quantum mechanics, especially superfluidity and superconductivity.

1.4 Superfluidity

Perhaps the most remarkable phenomenon related to ultracold temperatures is the *superfluidity* of a BEC. Superfluid is a fluid that flows without any friction. The most well known appearance of superfluidity happens in certain metals when cooled to temperatures of a few kelvins, where the conduction electrons of the metal enter a superfluid state and the metal becomes a superconductor, a conductor with no electric resistance. In fact superconductivity is

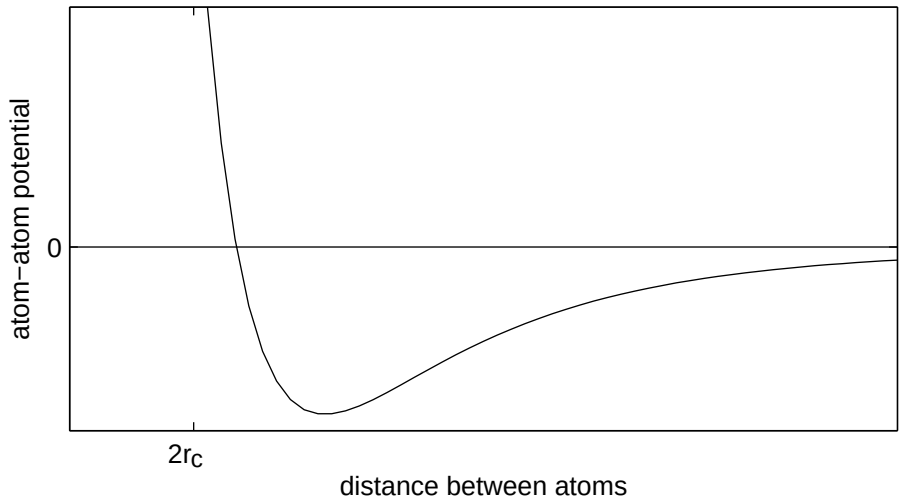

FIGURE 1.3: Schematic of a realistic model for the atom-atom potential with the van der Waals interaction. Here r_C is the hard core radius of an atom.

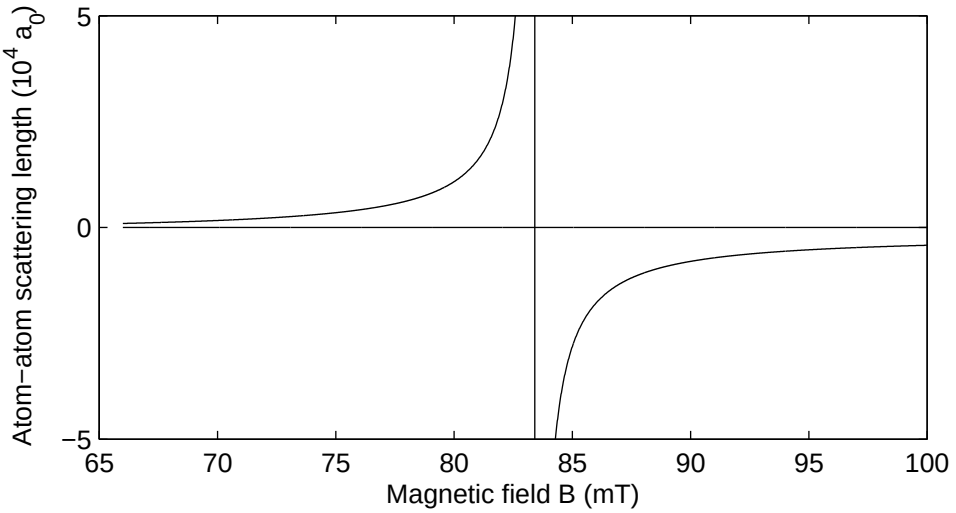

FIGURE 1.4: Atom-atom s-wave scattering length between the two lowest Zeeman sublevels of ^{6}Li, as a function of magnetic field, near a Feshbach resonance at 83.41 mT [9].

simply superfluidity of charged particles. Because superconducting materials have a vast number of applications, from electronics to mass transport, finding a theory to describe them completely is the Holy Grail of solid state physics. Although the superconductivity of conventional metals is well understood in terms of the theory by Bardeen, Cooper and Schrieffer (BCS) [10] and its extensions [11, 12, 13], the so called high temperature superconductivity [14, 15], exhibited by some ceramic compounds, continues to elude even qualitative descriptions on the microscopic level.

One motivation for studying atom gases is the possibility of understanding superconductivity better. However, as the charge carriers in solids are electrons, i.e. fermions, it makes sense to use the fermionic isotopes for these studies. Because fermions as such do not, by definition, form a BEC, their superfluidity is slightly more complicated. This phenomenon comes about by the formation of composite bosons, for which the condensation is possible. The most usual mechanism for this is pairing; as explained above, two fermionic particles together form a bosonic particle.

Because of the Pauli exclusion principle, it is not possible for two identical fermions in the same quantum state to form a pair. This is why experiments with fermionic isotopes are performed with a mixture of two different hyperfine states, allowing pairing between atoms in different states. There are two pairing mechanisms for the atoms. The simpler pairing mechanism is due to the interaction directly, as the potential always has bound states. Atoms in such a state are bound in space and form a molecule. The other pairing mechanism is the BCS paradigm, where fermions with a weak attractive interaction form non-local pairs, called Cooper pairs. While the molecule is simply a two-body state, the BCS state is a true many-body state where the pairs have lower energy than free particles due to interactions with all the other particles. A major part of this thesis deals with generalizations of the BCS pairing to more complicated systems.

The first evidence of molecules of ultracold fermionic atoms was reported in 2003 [16, 17, 18, 19] and later in the same year Bose condensates of these molecules were observed [20, 21, 22, 23]. The first experimental evidence of pairing on the attractive side of the resonance was shown in 2004 [24, 25, 26, 27]. The pairing gap was measured in the same year by radiofrequency spectroscopy [28, 29]. In 2005 the phase transition to a superfluid state was observed by measuring heat capacity as a function of temperature [30]. In the same year the MIT group observed quantized vortices in a cooled down sample of fermionic atoms, thereby proving that the sample was in a superfluid state [31].

Chapter 2

Optical lattices

2.1 The laser fields forming the lattice

An optical lattice is a one-, two-, or three-dimensional periodic potential for atoms, created with the use of counterpropagating laser beams. In order to discuss the physical properties of optical lattices, I will explain them from the point of view of classical electromagnetism. The electric field of a beam propagating in the x-direction is of the form

$$\mathbf{E}_0 A(r, \varphi) e^{i(kx-\omega t)}, \tag{2.1}$$

where r is the radial distance from the beam, φ is the polar angle, ω is the frequency of the beam, k is its wave number, $A(r, \varphi)$ is the amplitude of the beam, and $\mathbf{E}_0$ is a unit vector with dimensions V/m. Summing such a wave with another one, propagating to the opposite direction, gives a total field of

$$\mathbf{E}_0 A(r, \varphi) \left(e^{i(kx-\omega t)} + e^{i(-kx-\omega t)}\right) = 2\mathbf{E}_0 A(r, \varphi) e^{-i\omega t} \cos(kx), \tag{2.2}$$

which is a standing wave along the x-axis.

Though atoms themselves are electrically neutral, they do interact with external electric fields due to polarization. This means that an external field displaces the positively charged nucleus and the center of mass of the negatively charged electron cloud relative to each other, making the atom an electric dipole. The total electric force acting on an atomic dipole is [32]

$$\mathbf{F}(\mathbf{r}) = q\left(\mathbf{E}(\mathbf{r} + \frac{\delta\mathbf{r}}{2}) - \mathbf{E}(\mathbf{r} - \frac{\delta\mathbf{r}}{2})\right) \approx q\left(\frac{1}{2}\delta\mathbf{r} \cdot \nabla\mathbf{E}(\mathbf{r}) + \frac{1}{2}\delta\mathbf{r} \cdot \nabla\mathbf{E}(\mathbf{r})\right), \tag{2.3}$$

where q is the charge of the nucleus, $\mathbf{r}$ is the position of the atom, and $\delta\mathbf{r}$ is the relative displacement of the positive and negative charges. Noting that

$q\delta\mathbf{r} = \mathbf{p}$, the dipole moment of the atom, and assuming the polarization is linear, $\mathbf{p} = \alpha\mathbf{E}$, this is more clearly written as

$$\mathbf{F}(\mathbf{r}) = (\mathbf{p} \cdot \nabla)\mathbf{E}(\mathbf{r}) = \alpha(\mathbf{E}(\mathbf{r}) \cdot \nabla)\mathbf{E}(\mathbf{r}). \tag{2.4}$$

From standard vector calculus it follows that $(\mathbf{E} \cdot \nabla)\mathbf{E} = \frac{1}{2}\nabla\mathbf{E}^2 - \mathbf{E} \times \nabla \times \mathbf{E}$, and since $\nabla \times \mathbf{E} = -\partial\mathbf{B}/\partial t$, which averaged over time gives zero, it can be seen that the total force acting on the atom is proportional to the gradient of the square of the electric field. Therefore the atoms experience the standing electromagnetic wave created by the lasers as a potential of the form

$$V(\mathbf{r}) = -\alpha\frac{\mathbf{E}^2}{2} \propto I\cos^2(kx), \tag{2.5}$$

where the intensity $I = |A|^2$. Thus the laser beams act as a one-dimensional periodic potential for the polarizable atoms, with the period $d = \lambda/2$, where λ is the wavelength of the laser. Adding another such potential in an orthogonal direction makes the lattice potential two-dimensional, and adding a third one in the remaining orthogonal direction makes the lattice fully three-dimensional.

The sign of the atomic polarizability α depends on the frequency of the laser, compared to the transitions of the atom. If ω is slightly detuned from an atomic transition between states $|g\rangle$ and $|e\rangle$, with energy difference $\hbar\omega_0$, the polarizability is inversely proportional to $\hbar(\omega_0 - \omega)$ [33]. Thus, if the laser is blue detuned ($\omega > \omega_0$), $\alpha < 0$ and the atoms are attracted to the nodes of the field. Conversely, with a red detuned laser, where $\omega < \omega_0$, the polarizability is positive and the atoms are attracted to maxima of the field.

If all the angles between the lasers are 90° and the wavelengths identical, the lattice is a cubic lattice. Varying either the angles or some of the wavelengths yields different symmetries, but this study is limited to the case of a simple cubic lattice.

The energies in lattice experiments scale with the lattice recoil energy E_R,

$$E_R = \frac{\hbar^2 k_l^2}{2m}, \tag{2.6}$$

where k_l is the wavenumber of the laser and m is the mass of the atom. When discussing optical lattices, it is typical to give all energies in the units of the recoil energy. This is an extremely low energy scale. A typical experimental setup uses a 1064 nm laser with ^{6}Li atoms [34], which gives $E_R \approx 2 \cdot 10^{-29}$ J or 10^{-10} eV. The energy scale is therefore 10 orders of magnitude lower than the energy scales involved in the excitations of electrons in atoms.

2.2 Lattice potential and tunnelling

A simplistic view of the effect of the lattice potential on a single atom can be given as follows: the center of each lattice site resembles a harmonic oscillator potential, with a non-degenerate ground state. The wavefunction of an atom occupying this state is localized around the center and decays exponentially outside the lattice site. Depending on the depth of the lattice potential, usually denoted with $s \propto I$, the wavefunction has some overlap with the neighbouring sites, thereby allowing tunnelling between these sites. The lattice depths commonly employed in experiments are such that tunnelling further than the nearest neighbour is negligible, the atom is well localized in the lattice site. Band structures are given by the standard tight binding model [35], and the bandgap between the lowest band and the first excited band is much larger than the typical energies of the atoms in the systems.

Including interactions, the system is well described by the nearest-neighbour Hubbard model, with the interaction energy of two atoms occupying the same point-like lattice site being U and the energy associated with a single atom tunnelling to the next site J. The Hubbard model is widely used in the field of solid state physics, where the tunnelling energy is usually denoted with t.

2.2.1 Harmonic confinement

Since for a typical laser beam the intensity profile perpendicular to the direction of propagation is not constant, but rather a Gaussian function, $V(\mathbf{r})$ increases as $\mathbf{r}$ is further away from the center axis of the beam. This is both a blessing and a curse. Without this confinement, the lattice potential alone could not trap a cloud of atoms, but the atoms would escape by tunnelling away from the center, and thus this property makes experimental setups easier to construct. On the other hand, as the potential has neither the elliptical symmetry of a pure harmonic trap, nor the translational symmetry of a lattice, accurate theoretical models are difficult to create.

2.3 Measuring the momentum distribution

An important aspect of optical lattice experiments are the so called *time of flight* (TOF) measurements [33]. As the lattice Hamiltonian has translational invariance, according to the Bloch theorem [35], its eigenfunctions are of the form $u_{\mathbf{q}}(\mathbf{r})e^{i\mathbf{q}\cdot\mathbf{r}}$, where $u_{\mathbf{q}}(\mathbf{r})$ is a function with lattice periodicity. When the atoms are released from the lattice, i.e. the lattice is switched off nearly instantaneously, the wavefunction of an atom becomes a superposition of plane

waves with real momenta equal to

$$\mathbf{p}_n = \hbar\mathbf{q} + 2n\hbar\mathbf{k},$$

where n is an integer and $\mathbf{k}$ is a reciprocal lattice vector, with length $|\mathbf{k}| = 2\pi/\lambda$, where λ is the wavelength of the laser. The factor of 2 results from the fact that the lattice potential is of the form $\cos^2$, with a period equal to half the wavelength of the laser. After time t, the atom is at position

$$\mathbf{x}_n = \frac{\mathbf{p}_n}{m}t = \frac{\hbar\mathbf{q} + 2n\hbar\mathbf{k}}{m}t.$$

If an atom is detected at any of the equally spaced positions $\mathbf{x}_n$, it has had to come from the state with lattice momentum $\hbar\mathbf{q}$. This is often used as a tool to map the momentum distribution in a lattice to a position distribution, which can be measured with particle detectors.

In contrast, if the lattice potential is switched off adiabatically, i.e. slowly, its wavefunction retains only the plane wave part corresponding to $\mathbf{q}$. In this case each Bloch state is mapped onto a unique momentum state in free space, and a state in the nth band will be mapped to the nth Brillouin zone.

2.4 Experiments with fermions in optical lattices

Several interesting experiments have already been performed with fermionic atoms in optical lattices. One is the observation of fermionic superfluidity in an optical lattice, by the MIT group [34]. This experiment was done with a mixture of equal amounts of atoms in the two lowest hyperfine states of ^{6}Li. A cooled-down sample was loaded into a three-dimensional optical lattice and brought into the BCS-BEC crossover regime by using the Feshbach resonance centered at 834 G. In this strongly interacting regime the atoms form localized pairs, which were observed in the following way: the confining potential was switched off and an absorption image taken after a time of flight of 6.5 ms. The images show clear peaks at the locations corresponding to reciprocal lattice vectors, which proves that there was strong coherence through the sample. Strong coherence is characteristic for a superfluid, thereby proving the sample was in a superfluid state. Furthermore, the distance from the first order peaks to the zero-momentum peak corresponds to a pair of atoms carrying momentum equal to the reciprocal lattice vector. The experiment also demonstrated that increasing the lattice depth beyond $6E_R$ destroys this coherence. A simplified explanation is that atoms become strongly localized in the deep lattice sites.

The observation of superfluidity was preceded by experiments in the ETH Zürich in 2004 and 2005 [36, 37]. In the first experiment the group observed Fermi surfaces and demonstrated that the shape of the surface and its dependence on density corresponds to an ideal Fermi gas occupying the lowest Bloch band of a simple cubic lattice. In the latter experiment, molecule formation was observed and the binding energy of the molecules measured with radiofrequency spectroscopy. In a later experiment the ETH group explored the center of mass dynamics of a cloud of fermionic atoms in a lattice [38]. In the experiment the center of the harmonic trap (superimposed on the lattice as explained above) was displaced, causing the cloud to oscillate in the trap. It was found that the oscillation period depended on the interaction strength between the atoms; with strong interactions the oscillation was much slower. This can be understood with the following picture: weakly interacting atoms tunnel from site to site as single atoms with tunneling strength J, but strongly interacting atoms form pairs, which tunnel as a second order process, with effective tunneling rate J^2/U, where U is the interaction strength [39]. The most recent experiment reported by the same group is the observation of a fermionic Mott insulator [40]. This state is formed by repulsively interacting atoms with one atom in each lattice site. Because of the strong repulsive interaction, the energy cost of having two atoms in the same lattice site is large and therefore the system is in an incompressible state where tunnelling is suppressed. The experiment showed how the incompressibility of the system, the percentage of doubly occupied lattice sites, and the rise of a gapped mode in the excitation spectrum are connected, thereby confirming the observation of a fermionic Mott insulator.

The third group in the world to experiment with fermionic atoms in optical lattices so far is in Mainz, Germany. They observed strong anticorrelation peaks in the density-density correlation function of atomic shot noise from a Fermi gas released from an optical lattice [41]. Because fermions in a lattice occupy different Bloch states due to the Pauli exclusion principle, their momenta upon release assume values $\hbar q_1 + 2n_1\hbar k$ and $\hbar q_2 + 2n_2\hbar k$, where $q_1 \neq q_2$ and k is the lattice wavevector. Thus, after a time of flight t, their distance is $d = (q_1 - q_2 + 2k(n_1 - n_2))\hbar t/m$. The measured correlation function showed clear dips at distances which are integer multiples of $2k\hbar t/m$, as expected for a degenerate Fermi gas. This fermionic antibunching is a true quantum statistical phenomenon and the observation is a clear proof of the quantum nature of the system. This group has also reported on an experiment with repulsively interacting fermionic atoms in a lattice [42]. This experiment also showed evidence of the Mott insulating phase.

Chapter 3

Imbalanced pairing and superfluidity in optical lattices

The object of study in this work is a two-component atomic Fermi gas. Although the components do not represent different spin states *per se*, as discussed in chapter 1, they are usually referred to as spin up ($\uparrow$) and spin down ($\downarrow$) atoms. The many body Hamiltonian of the system is

$$\begin{aligned} H = &\sum_{\sigma=\uparrow,\downarrow} \int \psi_\sigma^\dagger(\mathbf{x}) \left(-\frac{\hbar^2}{2m}\nabla^2 + V_\sigma(\mathbf{x}) \right) \psi_\sigma(\mathbf{x})\, d^3\mathbf{x} \\ &+ \frac{1}{2} \int\int \psi_\uparrow^\dagger(\mathbf{x})\psi_\downarrow^\dagger(\mathbf{x}')U(\mathbf{x},\mathbf{x}')\psi_\downarrow(\mathbf{x}')\psi_\uparrow(\mathbf{x})\, d^3\mathbf{x}' d^3\mathbf{x}, \end{aligned} \tag{3.1}$$

where $\psi_\uparrow$ and $\psi_\downarrow$ are fermionic field operators, $V_\sigma(\mathbf{x})$ is the external potential felt by component σ, and $U(\mathbf{x},\mathbf{x}')$ is the two-body potential. This Hamiltonian already takes into account that three-body processes are extremely unlikely because of the diluteness of the gas and can thus be neglected.

The standard way to deal with the complex two-body interaction potential $U(\mathbf{x},\mathbf{x}')$ is to use an effective interaction where the details of the short wavelength part of the potential have been integrated out [43, 5]. In this approximation the potential takes the form

$$U(\mathbf{r}) = \frac{4\pi\hbar^2 a}{m}\delta(\mathbf{r}) \left[\frac{\partial}{\partial r}(r\cdot) \right]_{r=0}, \tag{3.2}$$

where $\mathbf{r}$ is the separation of the atoms, m is the mass of the atoms, and a is the s-wave scattering length. The interaction part therefore reduces to

$$\frac{2\pi\hbar^2 a}{m} \int \psi_\uparrow^\dagger(\mathbf{x})\psi_\downarrow^\dagger(\mathbf{x})\psi_\downarrow(\mathbf{x})\psi_\uparrow(\mathbf{x})\, d^3\mathbf{x}. \tag{3.3}$$

Finally the Hamiltonian has the form

$$\begin{aligned} H = \sum_{\sigma} \int \psi_{\sigma}^{\dagger}(\mathbf{x}) \left(-\frac{\hbar^2}{2m} \nabla^2 + V_{\sigma}(\mathbf{x}) \right) \psi_{\sigma}(\mathbf{x}) \, d^3\mathbf{x} \\ + \frac{1}{2} \frac{4\pi\hbar^2 a}{m} \int \psi_{\uparrow}^{\dagger}(\mathbf{x}) \psi_{\downarrow}^{\dagger}(\mathbf{x}) \psi_{\downarrow}(\mathbf{x}) \psi_{\uparrow}(\mathbf{x}) \, d^3\mathbf{x}. \end{aligned} \tag{3.4}$$

The lattice potential $V(\mathbf{x})$ is of the form $V_x \cos^2(k_x x) + V_y \cos^2(k_y y) + V_z \cos^2(k_z z)$. In the case of a single atom, the eigenfunctions of the lattice are Bloch wave functions [35]. The Bloch functions can be represented in the basis of Wannier functions that are localized in each lattice site. Thus the field operators can be expanded in the Wannier basis and keeping only the lowest vibrational states, the Hamiltonian can be written as the single-band Fermi-Hubbard Hamiltonian, given below [44].

3.1 Hubbard model

The Fermi-Hubbard Hamiltonian is

$$\begin{aligned} H - \mu_{\uparrow} N_{\uparrow} - \mu_{\downarrow} N_{\downarrow} = & - \sum_{n} \left(\mu_{\uparrow} \hat{c}_{\uparrow n}^{\dagger} \hat{c}_{\uparrow n} + \mu_{\downarrow} \hat{c}_{\downarrow n}^{\dagger} \hat{c}_{\downarrow n} \right) + U \sum_{n} \hat{c}_{\uparrow n}^{\dagger} \hat{c}_{\downarrow n}^{\dagger} \hat{c}_{\downarrow n} \hat{c}_{\uparrow n} \\ & - \sum_{\sigma \in \{\uparrow, \downarrow\}} \left(J_{\sigma x} \sum_{\langle n, m \rangle_x} + J_{\sigma y} \sum_{\langle n, m \rangle_y} + J_{\sigma z} \sum_{\langle n, m \rangle_z} \right) \hat{c}_{\sigma m}^{\dagger} \hat{c}_{\sigma n}, \end{aligned} \tag{3.5}$$

where n runs through all the lattice sites and $\langle \mathbf{n}, \mathbf{m} \rangle_x$ means a nearest neighbour pair in the x-direction, etc. The values of U and J are given by

$$\begin{aligned} U &= -\frac{8}{\sqrt{\pi}} \frac{a}{\lambda} \left(\frac{2 s_x s_y s_z E_R^3 \hbar^2}{m \lambda^2} \right)^{\frac{1}{4}} \\ J_{\sigma i} &= E_R e^{-\frac{\pi^2 \sqrt{s_i}}{4}} \left(\left(\frac{\pi^2 s_i}{4} - \frac{\sqrt{s_i}}{2} \right) - \frac{1}{2} s_i (1 + e^{-\sqrt{s_i}}) \right), \end{aligned} \tag{3.6}$$

where s_i is the lattice height in recoil energies in direction i and a is the "background" scattering length, i.e. the scattering length of the atoms in free space [45]. Here I have explicitly assumed that the potential experienced by the atoms does not depend on spin. This assumption does not change the functional form of the equations.

The full Hubbard Hamiltonian in three dimensions can only be solved for very small lattice sizes. In fact, since the size of the matrix representation of the Hamiltonian scales as 4^M, where M is the number of lattice sites, the full diagonalization for lattices with more than 12 sites is not feasible, regardless of the number of geometric dimensions. There are different ways to counter this limitation; this work uses the mean field approach. An arbitrary operator $\hat{A}$ can be written in the form $\hat{A} = \langle\hat{A}\rangle + \delta\hat{A}$, where $\delta\hat{A}$ represents fluctuations around the mean value, $\langle\hat{A}\rangle$. A product of two operators, $\hat{A}$ and $\hat{B}$, is therefore written as

$$\hat{A}\hat{B} = \left(\langle\hat{A}\rangle + \delta\hat{A}\right)\left(\langle\hat{B}\rangle + \delta\hat{B}\right) = \langle\hat{A}\rangle\langle\hat{B}\rangle + \langle\hat{A}\rangle\delta\hat{B} + \delta\hat{A}\langle\hat{B}\rangle + \delta\hat{A}\delta\hat{B} \tag{3.7}$$

Assuming the fluctuations to be small, the second order fluctuation term, $\delta\hat{A}\delta\hat{B}$, can be neglected. The exclusion of second order fluctuation terms is the core of the mean field approximation. This approach fails to give good results in a system where fluctuations are important and it can fail completely if the fluctuations play a dominant role, as is usually the case in one-dimensional systems [46]. Having thrown out the product of fluctuations, we can rewrite this as

$$\begin{aligned}\langle\hat{A}\rangle\langle\hat{B}\rangle + \langle\hat{A}\rangle\delta\hat{B} + \delta\hat{A}\langle\hat{B}\rangle &= \langle\hat{A}\rangle\langle\hat{B}\rangle + \langle\hat{A}\rangle\left(\hat{B} - \langle\hat{B}\rangle\right) + \left(\hat{A} - \langle\hat{A}\rangle\right)\langle\hat{B}\rangle \\ &= \langle\hat{A}\rangle\hat{B} + \hat{A}\langle\hat{B}\rangle - \langle\hat{A}\rangle\langle\hat{B}\rangle .\end{aligned} \tag{3.8}$$

We can now use this result for the four-operator product in (3.5) by $\hat{A} = \hat{c}^\dagger_{\uparrow\mathbf{n}}\hat{c}^\dagger_{\downarrow\mathbf{n}}$ and $\hat{B} = \hat{c}_{\downarrow\mathbf{n}}\hat{c}_{\uparrow\mathbf{n}}$ to get

$$\hat{c}^\dagger_{\uparrow\mathbf{n}}\hat{c}^\dagger_{\downarrow\mathbf{n}}\hat{c}_{\downarrow\mathbf{n}}\hat{c}_{\uparrow\mathbf{n}} = \hat{c}^\dagger_{\uparrow\mathbf{n}}\hat{c}^\dagger_{\downarrow\mathbf{n}}\langle\hat{c}_{\downarrow\mathbf{n}}\hat{c}_{\uparrow\mathbf{n}}\rangle + \langle\hat{c}^\dagger_{\uparrow\mathbf{n}}\hat{c}^\dagger_{\downarrow\mathbf{n}}\rangle\hat{c}_{\downarrow\mathbf{n}}\hat{c}_{\uparrow\mathbf{n}} - \langle\hat{c}^\dagger_{\uparrow\mathbf{n}}\hat{c}^\dagger_{\downarrow\mathbf{n}}\rangle\langle\hat{c}_{\downarrow\mathbf{n}}\hat{c}_{\uparrow\mathbf{n}}\rangle. \tag{3.9}$$

Now $U\langle\hat{c}^\dagger_{\uparrow\mathbf{n}}\hat{c}^\dagger_{\downarrow\mathbf{n}}\rangle$ is the order parameter of the mean field theory. As a second approximation let us assume its form is a plane wave,

$$U\langle\hat{c}^\dagger_{\uparrow\mathbf{n}}\hat{c}^\dagger_{\downarrow\mathbf{n}}\rangle = \Delta e^{-2i\mathbf{q}\cdot\mathbf{n}}, \tag{3.10}$$

where $\Delta \geqslant 0$. This is equivalent with the standard BCS-theory in the limit of $\mathbf{q} = 0$. This form of order parameter was first considered by Fulde and Ferrel [47] and Larkin and Ovchinnikov [48, 49]. The amplitude of the order parameter, Δ, plays a special role in the theory as the energy gap for quasiparticle excitations in the ground state of the system, as shown below.

The Hamiltonian is now in the form

$$\begin{aligned} H - \mu_\uparrow N_\uparrow - \mu_\downarrow N_\downarrow = &- \sum_{\mathbf{n}} \left(\mu_\uparrow \hat{c}^\dagger_{\uparrow\mathbf{n}} \hat{c}_{\uparrow\mathbf{n}} + \mu_\downarrow \hat{c}^\dagger_{\downarrow\mathbf{n}} \hat{c}_{\downarrow\mathbf{n}} \right) \\ &+ \sum_{\mathbf{n}} \left(\Delta e^{2i\mathbf{q}\cdot\mathbf{n}} \hat{c}^\dagger_{\uparrow\mathbf{n}} \hat{c}^\dagger_{\downarrow\mathbf{n}} + \Delta e^{-2i\mathbf{q}\cdot\mathbf{n}} \hat{c}_{\downarrow\mathbf{n}} \hat{c}_{\uparrow\mathbf{n}} - \frac{\Delta^2}{U} \right) \\ &- \sum_{\sigma} \sum_{\alpha\in\{x,y,z\}} J_{\sigma\alpha} \sum_{\langle \mathbf{n},\mathbf{m} \rangle_\alpha} \hat{c}^\dagger_{\sigma\mathbf{m}} \hat{c}_{\sigma\mathbf{n}}. \end{aligned} \tag{3.11}$$

It is convenient to write the Hamiltonian in the (quasi-)momentum representation, i.e. represent the operators in the plane wave basis. This essentially means doing a Fourier transform on (3.11) by

$$\begin{aligned} \hat{c}_{\uparrow\mathbf{n}} &= \frac{1}{\sqrt{M}} \sum_{\mathbf{k}} e^{i\mathbf{k}\cdot\mathbf{n}} \hat{c}_{\uparrow\mathbf{k}} \\ \hat{c}^\dagger_{\uparrow\mathbf{n}} &= \frac{1}{\sqrt{M}} \sum_{\mathbf{k}} e^{-i\mathbf{k}\cdot\mathbf{n}} \hat{c}^\dagger_{\uparrow\mathbf{k}} \\ \hat{c}_{\downarrow\mathbf{n}} &= \frac{1}{\sqrt{M}} \sum_{\mathbf{k}} e^{i\mathbf{k}\cdot\mathbf{n}} \hat{c}_{\downarrow\mathbf{k}} \\ \hat{c}^\dagger_{\downarrow\mathbf{n}} &= \frac{1}{\sqrt{M}} \sum_{\mathbf{k}} e^{-i\mathbf{k}\cdot\mathbf{n}} \hat{c}^\dagger_{\downarrow\mathbf{k}'} \end{aligned} \tag{3.12}$$

where M is the (finite) number of lattice sites and $\mathbf{k}$ runs through the reciprocal lattice. The density terms transform as

$$\begin{aligned} \sum_{\mathbf{n}} \hat{c}^\dagger_{\uparrow\mathbf{n}} \hat{c}_{\uparrow\mathbf{n}} &= \sum_{\mathbf{n}} \left(\frac{1}{\sqrt{M}} \sum_{\mathbf{k}} e^{-i\mathbf{k}\cdot\mathbf{n}} \hat{c}^\dagger_{\uparrow\mathbf{k}} \right) \left(\frac{1}{\sqrt{M}} \sum_{\mathbf{k}'} e^{i\mathbf{k}'\cdot\mathbf{n}} \hat{c}_{\uparrow\mathbf{k}'} \right) \\ &= \frac{1}{M} \sum_{\mathbf{n}} \sum_{\mathbf{k},\mathbf{k}'} e^{i(\mathbf{k}'-\mathbf{k})\cdot\mathbf{n}} \hat{c}^\dagger_{\uparrow\mathbf{k}} \hat{c}_{\uparrow\mathbf{k}'} = \sum_{\mathbf{k}} \hat{c}^\dagger_{\uparrow\mathbf{k}} \hat{c}_{\uparrow\mathbf{k}}, \end{aligned} \tag{3.13}$$

where the following identity is used:

$$\frac{1}{M} \sum_{\mathbf{n}} e^{i(\mathbf{k}'-\mathbf{k})\cdot\mathbf{n}} = \delta_{\mathbf{k},\mathbf{k}'}. \tag{3.14}$$

This equation holds for all reciprocal lattice vectors $\mathbf{k}, \mathbf{k}'$.

Similarly, the interaction term becomes

$$\begin{aligned}\sum_{\mathbf{n}}\left(\Delta e^{2i\mathbf{q}\cdot\mathbf{n}}\hat{c}^{\dagger}_{\uparrow\mathbf{n}}\hat{c}^{\dagger}_{\downarrow\mathbf{n}}\right) =& \frac{1}{M}\sum_{\mathbf{n},\mathbf{k},\mathbf{k}'}\left(\Delta e^{2i\mathbf{q}\cdot\mathbf{n}}e^{-i\mathbf{k}\cdot\mathbf{n}}\hat{c}^{\dagger}_{\uparrow\mathbf{k}}e^{-i\mathbf{k}'\cdot\mathbf{n}}\hat{c}^{\dagger}_{\downarrow\mathbf{k}'}\right)\\ =& \frac{1}{M}\sum_{\mathbf{n},\mathbf{k},\mathbf{k}'}\left(\Delta e^{i(2\mathbf{q}-\mathbf{k}-\mathbf{k}')\cdot\mathbf{n}}\hat{c}^{\dagger}_{\uparrow\mathbf{k}}\hat{c}^{\dagger}_{\downarrow\mathbf{k}'}\right)\\ =& \sum_{\mathbf{k},\mathbf{k}'}\underbrace{\left(\frac{1}{M}\sum_{\mathbf{n}}e^{i(2\mathbf{q}-\mathbf{k}-\mathbf{k}')\cdot\mathbf{n}}\right)}_{=\delta_{\mathbf{k}+\mathbf{k}',2\mathbf{q}}}\Delta\hat{c}^{\dagger}_{\uparrow\mathbf{k}}\hat{c}^{\dagger}_{\downarrow\mathbf{k}'}\\ =& \sum_{\mathbf{k}}\Delta\hat{c}^{\dagger}_{\uparrow\mathbf{k}+\mathbf{q}}\hat{c}^{\dagger}_{\downarrow-\mathbf{k}+\mathbf{q}}.\end{aligned} \tag{3.15}$$

The nearest neighbour hopping term gives rise to a cosine dispersion, for example the x-direction looks like

$$\begin{aligned}&\sum_{\langle\mathbf{n},\mathbf{m}\rangle_x}\left(\hat{c}^{\dagger}_{\uparrow\mathbf{m}}\hat{c}_{\uparrow\mathbf{n}}+\hat{c}^{\dagger}_{\downarrow\mathbf{m}}\hat{c}_{\downarrow\mathbf{n}}\right)\\ &=\sum_{\mathbf{n}}\left((\hat{c}^{\dagger}_{\uparrow\mathbf{n}+(1,0,0)}+\hat{c}^{\dagger}_{\uparrow\mathbf{n}-(1,0,0)})\hat{c}_{\uparrow\mathbf{n}}+(\hat{c}^{\dagger}_{\downarrow\mathbf{n}+(1,0,0)}+\hat{c}^{\dagger}_{\downarrow\mathbf{n}-(1,0,0)})\hat{c}_{\downarrow\mathbf{n}}\right)\\ &=\frac{1}{M}\sum_{\mathbf{n},\mathbf{k},\mathbf{k}'}e^{-i((\mathbf{k}-\mathbf{k}')\cdot\mathbf{n})}\underbrace{\left(e^{ik_x}+e^{-ik_x}\right)}_{=2\cos k_x}\left(\hat{c}^{\dagger}_{\uparrow\mathbf{k}}\hat{c}_{\uparrow\mathbf{k}'}+\hat{c}^{\dagger}_{\downarrow\mathbf{k}}\hat{c}_{\downarrow\mathbf{k}'}\right)\\ &=\sum_{\mathbf{k}}2\cos k_x\left(\hat{c}^{\dagger}_{\uparrow\mathbf{k}}\hat{c}_{\uparrow\mathbf{k}}+\hat{c}^{\dagger}_{\downarrow\mathbf{k}}\hat{c}_{\downarrow\mathbf{k}}\right).\end{aligned} \tag{3.16}$$

Finally, we have arrived at the mean field Hubbard Hamiltonian in momentum space,

$$\begin{aligned}\widehat{H}=\sum_{\mathbf{k}}\Big(&\xi_{\uparrow\mathbf{k}}\hat{c}^{\dagger}_{\uparrow\mathbf{k}}\hat{c}_{\uparrow\mathbf{k}}+\xi_{\downarrow\mathbf{k}}\hat{c}^{\dagger}_{\downarrow\mathbf{k}}\hat{c}_{\downarrow\mathbf{k}}\\ &+\Delta\hat{c}^{\dagger}_{\uparrow\mathbf{k}+\mathbf{q}}\hat{c}^{\dagger}_{\downarrow-\mathbf{k}+\mathbf{q}}+\Delta\hat{c}_{\downarrow-\mathbf{k}+\mathbf{q}}\hat{c}_{\uparrow\mathbf{k}+\mathbf{q}}\Big)-\frac{\Delta^2}{U},\end{aligned} \tag{3.17}$$

where $\xi_{\sigma\mathbf{k}}=\epsilon_{\sigma\mathbf{k}}-\mu_\sigma=\sum_\alpha 2J_{\sigma\alpha}(1-\cos(k_\alpha))-\mu_\sigma$. Note that in order to get the dispersion correspond to that of a free particle in the limit of small k, the following terms have been added to the Hamiltonian:

$$2\sum_{\alpha}\sum_{\mathbf{k}}\left(J_{\sigma\alpha}\hat{c}^{\dagger}_{\sigma\mathbf{k}}\hat{c}_{\sigma\mathbf{k}}\right)=\sum_{\alpha}2J_{\sigma\alpha}N_\sigma. \tag{3.18}$$

3.2 Bogoliubov transformation

The Hamiltonian in (3.17) can be written in an equivalent form as

$$\begin{aligned}\widehat{H} = \sum_{\mathbf{k}} \Big(& \xi_{\uparrow \mathbf{k}+\mathbf{q}} \hat{c}^{\dagger}_{\uparrow \mathbf{k}+\mathbf{q}} \hat{c}_{\uparrow \mathbf{k}+\mathbf{q}} + \xi_{\downarrow -\mathbf{k}+\mathbf{q}} (1 - \hat{c}_{\downarrow -\mathbf{k}+\mathbf{q}} \hat{c}^{\dagger}_{\downarrow -\mathbf{k}+\mathbf{q}}) \\ & + \Delta \hat{c}^{\dagger}_{\uparrow \mathbf{k}+\mathbf{q}} \hat{c}^{\dagger}_{\downarrow -\mathbf{k}+\mathbf{q}} + \Delta \hat{c}_{\downarrow -\mathbf{k}+\mathbf{q}} \hat{c}_{\uparrow \mathbf{k}+\mathbf{q}} \Big) - \frac{\Delta^2}{U}.\end{aligned} \tag{3.19}$$

Now the operator part can be expressed as a matrix:

$$\begin{aligned}& \sum_{\mathbf{k}} \Big(\xi_{\uparrow \mathbf{k}+\mathbf{q}} \hat{c}^{\dagger}_{\uparrow \mathbf{k}+\mathbf{q}} \hat{c}_{\uparrow \mathbf{k}+\mathbf{q}} - \xi_{\downarrow -\mathbf{k}+\mathbf{q}} \hat{c}_{\downarrow -\mathbf{k}+\mathbf{q}} \hat{c}^{\dagger}_{\downarrow -\mathbf{k}+\mathbf{q}} \\ & + \Delta \hat{c}^{\dagger}_{\uparrow \mathbf{k}+\mathbf{q}} \hat{c}^{\dagger}_{\downarrow -\mathbf{k}+\mathbf{q}} + \Delta \hat{c}_{\downarrow -\mathbf{k}+\mathbf{q}} \hat{c}_{\uparrow \mathbf{k}+\mathbf{q}} \Big) = \\ & \sum_{\mathbf{k}} \begin{pmatrix} \hat{c}^{\dagger}_{\uparrow \mathbf{k}+\mathbf{q}} & \hat{c}_{\downarrow -\mathbf{k}+\mathbf{q}} \end{pmatrix} \begin{pmatrix} \xi_{\uparrow \mathbf{k}+\mathbf{q}} & \Delta \\ \Delta & -\xi_{\downarrow -\mathbf{k}+\mathbf{q}} \end{pmatrix} \begin{pmatrix} \hat{c}_{\uparrow \mathbf{k}+\mathbf{q}} \\ \hat{c}^{\dagger}_{\downarrow -\mathbf{k}+\mathbf{q}} \end{pmatrix}.\end{aligned} \tag{3.20}$$

The essential point in this representation is that it is a sum of independent 2×2 matrices that can be diagonalized separately. It is due to this feature that the mean field approach under discussion is the most simple and straightforward way to address superfluidity in a lattice theoretically.

Let us now derive a Bogoliubov transformation, B, for the terms of (3.20). The requirements are that B diagonalizes the matrix and that B is canonical, i.e. it preserves the fermionic anticommutation relations. Without any loss of generality B can be assumed real in this case. Denoting the new basis operators as $\hat{\gamma}_+$ and $\hat{\gamma}_-$, we have

$$\begin{pmatrix} \hat{\gamma}_{+,\mathbf{k}} \\ \hat{\gamma}^{\dagger}_{-,\mathbf{k}} \end{pmatrix} = B \begin{pmatrix} \hat{c}_{\uparrow \mathbf{k}+\mathbf{q}} \\ \hat{c}^{\dagger}_{\downarrow -\mathbf{k}+\mathbf{q}} \end{pmatrix} = \begin{pmatrix} B_{11} \hat{c}_{\uparrow \mathbf{k}+\mathbf{q}} + B_{12} \hat{c}^{\dagger}_{\downarrow -\mathbf{k}+\mathbf{q}} \\ B_{21} \hat{c}_{\uparrow \mathbf{k}+\mathbf{q}} + B_{22} \hat{c}^{\dagger}_{\downarrow -\mathbf{k}+\mathbf{q}} \end{pmatrix} \tag{3.21}$$

and we require

$$B \begin{pmatrix} \xi_{\uparrow \mathbf{k}+\mathbf{q}} & \Delta \\ \Delta & -\xi_{\downarrow -\mathbf{k}+\mathbf{q}} \end{pmatrix} B^{-1} = \begin{pmatrix} E_{+,\mathbf{k},\mathbf{q}} & 0 \\ 0 & -E_{-,\mathbf{k},\mathbf{q}} \end{pmatrix}. \tag{3.22}$$

It should be pointed out that the sign in front of E_- is a choice of notation at this point and does not affect the results. From the anticommutation relations it follows that

$$\begin{aligned} 1 &= \{\hat{\gamma}_{+,\mathbf{k}}, \hat{\gamma}^{\dagger}_{+,\mathbf{k}}\} = \{B_{11} \hat{c}_{\uparrow} + B_{12} \hat{c}^{\dagger}_{\downarrow}, B_{11} \hat{c}^{\dagger}_{\uparrow} + B_{12} \hat{c}_{\downarrow}\} = B_{11}^2 + B_{12}^2 \\ 1 &= \{\hat{\gamma}_{-,\mathbf{k}}, \hat{\gamma}^{\dagger}_{-,\mathbf{k}}\} = \{B_{21} \hat{c}^{\dagger}_{\uparrow} + B_{22} \hat{c}_{\downarrow}, B_{21} \hat{c}_{\uparrow} + B_{22} \hat{c}^{\dagger}_{\downarrow}\} = B_{21}^2 + B_{22}^2 \\ 0 &= \{\hat{\gamma}_{+,\mathbf{k}}, \hat{\gamma}_{-,\mathbf{k}}\} = \{B_{11} \hat{c}_{\uparrow} + B_{12} \hat{c}^{\dagger}_{\downarrow}, B_{21} \hat{c}^{\dagger}_{\uparrow} + B_{22} \hat{c}_{\downarrow}\} = B_{11} B_{21} + B_{12} B_{22}. \end{aligned} \tag{3.23}$$

These conditions imply $B_{11}^2 = B_{22}^2$, $B_{12}^2 = B_{21}^2$, and $B_{11}B_{21} + B_{12}B_{22} = 0$, which has several physically equivalent solutions that differ only by the locations of minus signs. It is now possible to choose

$$B = \begin{pmatrix} u & -v \\ v & u \end{pmatrix}, \tag{3.24}$$

where $u, v \in \mathbb{R}$ and $u^2 + v^2 = 1$. This form satisfies all the requirements given above. Because B is a unitary matrix, it is enough to solve the eigenvalue problem of the Hamiltonian and the columns of B are the eigenvectors. The eigenvalues are

$$\lambda_\pm = \frac{\xi_{\uparrow \mathbf{k}+\mathbf{q}} - \xi_{\downarrow -\mathbf{k}+\mathbf{q}}}{2} \pm \sqrt{\left(\frac{\xi_{\uparrow \mathbf{k}+\mathbf{q}} + \xi_{\downarrow -\mathbf{k}+\mathbf{q}}}{2}\right)^2 + \Delta^2}, \tag{3.25}$$

and therefore

$$E_{\pm,\mathbf{k}} = E_\mathbf{k} \pm \frac{\delta\xi_\mathbf{k}}{2} := \sqrt{\left(\frac{\xi_{\uparrow \mathbf{k}+\mathbf{q}} + \xi_{\downarrow -\mathbf{k}+\mathbf{q}}}{2}\right)^2 + \Delta^2} \pm \frac{\xi_{\uparrow \mathbf{k}+\mathbf{q}} - \xi_{\downarrow -\mathbf{k}+\mathbf{q}}}{2}. \tag{3.26}$$

For comparison with the standard BCS theory it is good to note that if both species experience the same potential, i.e. the single particle dispersions are identical, $\epsilon_{\uparrow\mathbf{k}} = \epsilon_\mathbf{k} = \epsilon_{\downarrow\mathbf{k}}$, and in addition $\mathbf{q} = 0$, this reduces to

$$E_{\pm,\mathbf{k}} = \sqrt{\left(\epsilon_\mathbf{k} - \frac{\mu_\uparrow + \mu_\downarrow}{2}\right)^2 + \Delta^2} \pm \frac{\mu_\downarrow - \mu_\uparrow}{2}. \tag{3.27}$$

When $\mu_\uparrow = \mu_\downarrow$, the minimum value of both E_+ and E_- is Δ, which shows that quasiparticle excitations have a minimum energy, i.e. energy gap, the magnitude of which is Δ.

For further applications, it is relevant to know the values of u^2, v^2, and uv; they are

$$\begin{aligned} u_\mathbf{k}^2 &= \frac{1}{2}\left(1 + \frac{\xi_{\uparrow \mathbf{k}+\mathbf{q}} + \xi_{\downarrow -\mathbf{k}+\mathbf{q}}}{2E_\mathbf{k}}\right) \\ v_\mathbf{k}^2 &= \frac{1}{2}\left(1 - \frac{\xi_{\uparrow \mathbf{k}+\mathbf{q}} + \xi_{\downarrow -\mathbf{k}+\mathbf{q}}}{2E_\mathbf{k}}\right) \\ u_\mathbf{k} v_\mathbf{k} &= -\frac{\Delta}{2E_\mathbf{k}}. \end{aligned} \tag{3.28}$$

The Hamiltonian can now be written in the form

$$\widehat{H} = \sum_\mathbf{k} \left(\begin{pmatrix} \hat{\gamma}_{+,\mathbf{k}}^\dagger & \hat{\gamma}_{-,\mathbf{k}} \end{pmatrix} \begin{pmatrix} E_{+,\mathbf{k}} & 0 \\ 0 & -E_{-,\mathbf{k}} \end{pmatrix} \begin{pmatrix} \hat{\gamma}_{+,\mathbf{k}} \\ \hat{\gamma}_{-,\mathbf{k}}^\dagger \end{pmatrix} + \xi_{\downarrow -\mathbf{k}+\mathbf{q}} \right) - \frac{\Delta^2}{U}, \tag{3.29}$$

with $E_\pm$ defined in (3.26). The operators $\hat{\gamma}_\pm$ are called quasiparticle operators. The idea of the quasiparticle picture is that whereas the original system is composed of real particles which interact, and therefore do not occupy energy eigenstates, the Bogoliubov transformation gives an equivalent Hamiltonian that describes non-interacting quasiparticles. The quasiparticles, although not actual particles in the traditional sense (they are in fact superpositions of a particle of one species and a hole of the other), behave like fermions because the anticommutation relations are preserved by the canonical transformation. Thus the system is now described as an ideal Fermi gas with dispersions given by E_+ and E_-:

$$\widehat{H} = \sum_{\mathbf{k}} \left(E_{+,\mathbf{k}} \hat{\gamma}^\dagger_{+,\mathbf{k}} \hat{\gamma}_{+,\mathbf{k}} + E_{-,\mathbf{k}} \hat{\gamma}^\dagger_{-,\mathbf{k}} \hat{\gamma}_{-,\mathbf{k}} + \xi_{\downarrow -\mathbf{k}+\mathbf{q}} - E_{-,\mathbf{k}} \right) - \frac{\Delta^2}{U}, \tag{3.30}$$

where the additional E_- appears because of the normal ordering.

3.3 Self-consistent crossover equations

It is now possible to derive a set of equations from which Δ, $\mu_\uparrow$, and $\mu_\downarrow$ can be solved. These equations are called crossover equations. To start with the number equations, note that the following holds for the total number of particles in either one of the spin components: $N_\sigma = \sum_{\mathbf{k}} \left\langle \hat{c}^\dagger_{\sigma,\mathbf{k}} \hat{c}_{\sigma,\mathbf{k}} \right\rangle$. It is straightforward to use the inverse of the Bogoliubov transformation U to write the particle operators as linear combinations of the quasiparticle operators as

$$\begin{aligned} \begin{pmatrix} \hat{c}_{\uparrow \mathbf{k}+\mathbf{q}} \\ \hat{c}^\dagger_{\downarrow -\mathbf{k}+\mathbf{q}} \end{pmatrix} &= B^{-1} \begin{pmatrix} \hat{\gamma}_{+,\mathbf{k}} \\ \hat{\gamma}^\dagger_{-,\mathbf{k}} \end{pmatrix} = B^\dagger \begin{pmatrix} \hat{\gamma}_{+,\mathbf{k}} \\ \hat{\gamma}^\dagger_{-,\mathbf{k}} \end{pmatrix} \\ &= \begin{pmatrix} u_{\mathbf{k}} & v_{\mathbf{k}} \\ -v_{\mathbf{k}} & u_{\mathbf{k}} \end{pmatrix} \begin{pmatrix} \hat{\gamma}_{+,\mathbf{k}} \\ \hat{\gamma}^\dagger_{-,\mathbf{k}} \end{pmatrix} = \begin{pmatrix} u_{\mathbf{k}} \hat{\gamma}_{+,\mathbf{k}} + v_{\mathbf{k}} \hat{\gamma}^\dagger_{-,\mathbf{k}} \\ u_{\mathbf{k}} \hat{\gamma}^\dagger_{-,\mathbf{k}} - v_{\mathbf{k}} \hat{\gamma}_{+,\mathbf{k}} \end{pmatrix}. \end{aligned} \tag{3.31}$$

Thus we arrive at

$$\begin{aligned} N_\uparrow &= \sum_k \left\langle \hat{c}^\dagger_{\uparrow k} \hat{c}_{\uparrow k} \right\rangle = \sum_k \left\langle \hat{c}^\dagger_{\uparrow k+q} \hat{c}_{\uparrow k+q} \right\rangle \\ &= \sum_k \left\langle \left(u_k \hat{\gamma}^\dagger_{+,k} + v_k \hat{\gamma}_{-,k} \right) \left(u_k \hat{\gamma}_{+,k} + v_k \hat{\gamma}^\dagger_{-,k} \right) \right\rangle \\ &= \sum_k \left\langle u_k^2 \hat{\gamma}^\dagger_{+,k} \hat{\gamma}_{+,k} + v_k^2 \hat{\gamma}_{-,k} \hat{\gamma}^\dagger_{-,k} + u_k v_k \hat{\gamma}_{-,k} \hat{\gamma}_{+,k} + u_k v_k \hat{\gamma}^\dagger_{+,k} \hat{\gamma}^\dagger_{-,k} \right\rangle \\ &= \sum_k u_k^2 \left\langle \hat{\gamma}^\dagger_{+,k} \hat{\gamma}_{+,k} \right\rangle + v_k^2 \left\langle \hat{\gamma}_{-,k} \hat{\gamma}^\dagger_{-,k} \right\rangle \\ &= \sum_k u_k^2 n_F(E_{+,k}) + v_k^2 n_F(-E_{-,k}). \end{aligned} \tag{3.32}$$

Note that expectation values of type $\langle \hat{\gamma}_{+,k} \hat{\gamma}_{-,k} \rangle$ are automatically zero. A similar equation holds for the number of down particles:

$$\begin{aligned} N_\downarrow &= \sum_k \left\langle \hat{c}^\dagger_{\downarrow k} \hat{c}_{\downarrow k} \right\rangle \\ &= \sum_k \left\langle \left(u_k \hat{\gamma}^\dagger_{-,k} - v_k \hat{\gamma}_{+,k} \right) \left(u_k \hat{\gamma}_{-,k} - v_k \hat{\gamma}^\dagger_{+,k} \right) \right\rangle \\ &= \sum_k u_k^2 \left\langle \hat{\gamma}^\dagger_{-,k} \hat{\gamma}_{-,k} \right\rangle + v_k^2 \left\langle \hat{\gamma}_{+,k} \hat{\gamma}^\dagger_{+,k} \right\rangle \\ &= \sum_k u_k^2 n_F(E_{-,k}) + v_k^2 n_F(-E_{+,k}). \end{aligned} \tag{3.33}$$

Using the original definition of the order parameter, $U\langle \hat{c}^\dagger_{\uparrow n} \hat{c}^\dagger_{\downarrow n} \rangle = \Delta e^{-2iq\cdot n}$, it

is possible to derive the so called *gap equation*:

$$\begin{aligned}
\frac{\Delta e^{-2i\mathbf{q}\cdot\mathbf{n}}}{U} &= \left\langle \hat{c}^\dagger_{\uparrow\mathbf{n}}\hat{c}^\dagger_{\downarrow\mathbf{n}} \right\rangle = \left\langle \sum_{\mathbf{k},\mathbf{k}'} e^{-i(\mathbf{k}+\mathbf{k}')\cdot\mathbf{n}}\hat{c}^\dagger_{\uparrow\mathbf{k}}\hat{c}^\dagger_{\downarrow\mathbf{k}'} \right\rangle \\
&= \left\langle \sum_{\mathbf{k},\mathbf{k}'} e^{-i(\mathbf{k}+\mathbf{k}')\cdot\mathbf{n}} \left(u_{\mathbf{k}-\mathbf{q}}\hat{\gamma}^\dagger_{+,\mathbf{k}-\mathbf{q}} + v_{\mathbf{k}-\mathbf{q}}\hat{\gamma}_{-,\mathbf{k}-\mathbf{q}} \right) \cdot \right. \\
&\quad \left. \left(-v_{-\mathbf{k}'+\mathbf{q}}\hat{\gamma}_{+,-\mathbf{k}'+\mathbf{q}} + u_{-\mathbf{k}'+\mathbf{q}}\hat{\gamma}^\dagger_{-,-\mathbf{k}'+\mathbf{q}} \right) \right\rangle \\
&= \sum_{\mathbf{k},\mathbf{k}'} e^{-i(\mathbf{k}+\mathbf{k}')\cdot\mathbf{n}} \left(- u_{\mathbf{k}-\mathbf{q}}v_{-\mathbf{k}'+\mathbf{q}} \underbrace{\left\langle \hat{\gamma}^\dagger_{+,\mathbf{k}-\mathbf{q}}\hat{\gamma}_{+,-\mathbf{k}'+\mathbf{q}} \right\rangle}_{\propto\delta_{\mathbf{k}',-\mathbf{k}+2\mathbf{q}}} \right. \\
&\quad \left. + u_{-\mathbf{k}'+\mathbf{q}}v_{\mathbf{k}-\mathbf{q}} \underbrace{\left\langle \hat{\gamma}_{-,\mathbf{k}-\mathbf{q}}\hat{\gamma}^\dagger_{-,-\mathbf{k}'+\mathbf{q}} \right\rangle}_{\propto\delta_{\mathbf{k}',-\mathbf{k}+2\mathbf{q}}} \right) \\
&= e^{-2i\mathbf{q}\cdot\mathbf{n}} \sum_{\mathbf{k}} u_{\mathbf{k}-\mathbf{q}}v_{\mathbf{k}-\mathbf{q}} \left(1 - n_F(E_{+,\mathbf{k}-\mathbf{q}}) - n_F(E_{-,\mathbf{k}-\mathbf{q}})\right).
\end{aligned} \tag{3.34}$$

Finally, in the limit of $\mathbf{q} = 0$, after substituting $-\Delta/2E_\mathbf{k}$ for uv and dividing by Δ, the gap equation is

$$1 = -U \sum_{\mathbf{k}} \frac{1 - n_F(E_{+,\mathbf{k}}) - n_F(E_{-,\mathbf{k}})}{2E_\mathbf{k}}. \tag{3.35}$$

Since U was defined as negative, the prefactor on the right hand side of the equation is positive.

The number equations (3.32) and (3.33), and the gap equation (3.35) together are equivalent with the standard BCS-Leggett theory. In the balanced case, where $N_\uparrow = N_\downarrow$, it is possible to choose $\mu_\uparrow = \mu_\downarrow$ by hand and eliminate one of the number equations. If the interactions are weak, i.e. $|U|$ is small, the chemical potential can be approximated with the Fermi energy. However, when the interaction strength increases, the chemical potential has to be solved from the number equation in order to get the correct results.

The calculation becomes more involved once non-zero values for $\mathbf{q}$ are allowed. In this case it is more feasible to solve Δ and $\mathbf{q}$ by minimizing the relevant free energy, as described in the next section.

3.4 Thermodynamics

To derive thermodynamical quantities of a physical system we need a partition function describing the system. In this case we use the grand canonical partition function,

$$Z_G = \mathrm{Tr} e^{-\beta \widehat{H}} = \sum_{\gamma} \langle \gamma | e^{-\beta \widehat{H}} | \gamma \rangle, \tag{3.36}$$

where the sum goes through the quasiparticle basis (i.e. the basis where the quasiparticle occupation numbers are good quantum numbers) of the Hilbert space and $\beta = 1/k_B T$. The Hamiltonian is of the form

$$\widehat{H} = \sum_{\mathbf{k}} \left(E_{+,\mathbf{k}} \hat{\gamma}^{\dagger}_{+,\mathbf{k}} \hat{\gamma}_{+,\mathbf{k}} + E_{-,\mathbf{k}} \hat{\gamma}^{\dagger}_{-,\mathbf{k}} \hat{\gamma}_{-,\mathbf{k}} \right) + C, \tag{3.37}$$

where $C = \sum_{\mathbf{k}} (\xi_{\downarrow -\mathbf{k}+\mathbf{q}} - E_{-,\mathbf{k}}) - \Delta^2/U$. As a constant, C is factored out of the expectation value and we get

$$Z_G = e^{-\beta C} \sum_{\gamma} \langle \gamma | e^{-\beta \sum_{\mathbf{k}} \left(E_{+,\mathbf{k}} \hat{\gamma}^{\dagger}_{+,\mathbf{k}} \hat{\gamma}_{+,\mathbf{k}} + E_{-,\mathbf{k}} \hat{\gamma}^{\dagger}_{-,\mathbf{k}} \hat{\gamma}_{-,\mathbf{k}} \right)} | \gamma \rangle. \tag{3.38}$$

Let us denote $\hat{n}_{+,\mathbf{k}} = \hat{\gamma}^{\dagger}_{+,\mathbf{k}} \hat{\gamma}_{+,\mathbf{k}}$ and $\hat{n}_{-,\mathbf{k}} = \hat{\gamma}^{\dagger}_{-,\mathbf{k}} \hat{\gamma}_{-,\mathbf{k}}$. Since the Hamiltonian is diagonal in quasiparticle representation, all commutators between $\hat{n}_{\pm,\mathbf{k}}$ and $\hat{n}_{\pm,\mathbf{k}'}$ are zero for all $\mathbf{k}, \mathbf{k}'$ and the exponential of the sum can be written as a product of exponentials,

$$Z_G = e^{-\beta C} \sum_{\gamma} \langle \gamma | \prod_{\mathbf{k}} e^{-\beta E_{+,\mathbf{k}} \hat{n}_{+,\mathbf{k}}} e^{-\beta E_{-,\mathbf{k}} \hat{n}_{-,\mathbf{k}}} | \gamma \rangle. \tag{3.39}$$

Because the quasiparticle occupation numbers are well defined in each state $|\gamma\rangle$, it holds that $e^{-\beta E_{\pm,\mathbf{k}} \hat{n}_{\pm,\mathbf{k}}} |\gamma\rangle = e^{-\beta E_{\pm,\mathbf{k}} n_{\pm,\mathbf{k},\gamma}} |\gamma\rangle$, where $n_{\pm,\mathbf{k},\gamma}$ stands for the occupation number of a quasiparticle of type $\pm$ in state $\mathbf{k}$ in $|\gamma\rangle$. Thus the partition function is

$$Z_G = e^{-\beta C} \sum_{\gamma} \prod_{\mathbf{k}} e^{-\beta E_{+,\mathbf{k}} n_{+,\mathbf{k},\gamma}} e^{-\beta E_{-,\mathbf{k}} n_{-,\mathbf{k},\gamma}}. \tag{3.40}$$

The sum over γ runs through every combination of possible occupation numbers exactly once. Therefore this can be written as a product of sums over different occupation numbers for state $\mathbf{k}$:

$$Z_G = e^{-\beta C} \prod_{\mathbf{k}} \left(\sum_{n_{+,\mathbf{k}}} e^{-\beta E_{+,\mathbf{k}} n_{+,\mathbf{k}}} \right) \left(\sum_{n_{-,\mathbf{k}}} e^{-\beta E_{-,\mathbf{k}} n_{-,\mathbf{k}}} \right). \tag{3.41}$$

Since the quasiparticles are fermions, the possible occupation numbers for a given $\mathbf{k}$-state are 0 and 1, giving

$$Z_G = e^{-\beta C} \prod_{\mathbf{k}} \left(1 + e^{-\beta E_{+,\mathbf{k}}}\right) \left(1 + e^{-\beta E_{-,\mathbf{k}}}\right). \tag{3.42}$$

Thus the thermodynamic grand potential is

$$\Omega = -\frac{1}{\beta} \ln Z_G = -\frac{1}{\beta} \ln \left(e^{-\beta C} \prod_{\mathbf{k}} \left(1 + e^{-\beta E_{+,\mathbf{k}}}\right) \left(1 + e^{-\beta E_{-,\mathbf{k}}}\right) \right), \tag{3.43}$$

which reduces to

$$\Omega = -\frac{\Delta^2}{U} + \sum_{\mathbf{k}} \left(\xi_{\downarrow -\mathbf{k}+\mathbf{q}} - E_{-,\mathbf{k}} - \frac{1}{\beta} \ln \left(\left(1 + e^{-\beta E_{+,\mathbf{k}}}\right) \left(1 + e^{-\beta E_{-,\mathbf{k}}}\right) \right) \right). \tag{3.44}$$

The core of the (mean field) theory of phase transitions is as follows: the free energy of the system depends on the order parameter, and in thermodynamic equilibrium the order parameter takes the value that minimizes the free energy. For the normal gas-liquid-solid -type situation, the order parameter is density, and temperature and pressure are fixed parameters. For a dilute Fermi gas in an optical trap, described by the theory presented here, the order parameter is 4-dimensional: Δ is the amplitude and $\mathbf{q}$ gives the magnitude and direction of the wave vector in the plane wave form. The fixed parameters are temperature, and depending on the situation, either the chemical potentials $\mu_\uparrow$ and $\mu_\downarrow$ or the total particle numbers, $N_\uparrow$ and $N_\downarrow$, as explained below.

Because the gas is trapped in a harmonic trap and is not in a particle bath, the total particle numbers, $N_\uparrow$ and $N_\downarrow$ are constant in the experiment. Since the time scale of spin relaxation is much larger than the time scale of the experiment, the atoms are prevented from converting their spin. In this situation the atom distribution assumes a form where the chemical potential is a constant throughout the trap. The grand potential $\Omega(\Delta, \mathbf{q}, \mu_\uparrow, \mu_\downarrow)$ is considered to depend directly on $\mu_\uparrow$ and $\mu_\downarrow$ and is therefore the energy to minimize when the local particle number is not fixed. Such a situation rises naturally for example when using the local density approximation (LDA), covered below.

There are situations where it is viable to consider the particle density of the system to be homogeneous, such as a very shallow trap, or a higher order trap, which more closely resembles a box. In this case $\mu_\uparrow$ and $\mu_\downarrow$ are no longer fixed and the relevant thermodynamic quantity to minimize is the Helmholtz free energy F. This can be calculated from the grand potential with

$$F = \Omega + \mu_\uparrow n_\uparrow + \mu_\downarrow n_\downarrow, \tag{3.45}$$

where $n_\uparrow$ and $n_\downarrow$ are numbers of atoms per lattice site. These quantities are often called filling fractions or filling factors. Because of the single band model, it is not possible to have more than one atom of one species in a single lattice site and thus the filling factors are bounded between 0 and 1. When minimizing F it is important to take care that the chemical potentials satisfy the number equations (3.32) and (3.33). Numerically this means that for every $(\Delta, \mathbf{q})$ -pair, before the value of F can be calculated, the number equations must be solved first. Since in the interacting case $\mu_\uparrow$ and $\mu_\downarrow$ are not independent, and the value of $\mu_\uparrow$ affects the correct value of $\mu_\downarrow$ and vice versa, the equations have to be solved iteratively until both chemical potentials have converged. This process actually takes the bulk of the computation time needed by the multi-dimensional minimization of F.

There are three qualitatively different values for $(\Delta, \mathbf{q})$, namely $(\Delta > 0, \mathbf{q} = 0)$, $(\Delta > 0, |\mathbf{q}| > 0)$, and $(\Delta = 0)$.

It can be said that the situation where $\Delta > 0$ and $\mathbf{q} = 0$ represents two phases, depending on the polarization P, defined as

$$P = \frac{n_\uparrow - n_\downarrow}{n_\uparrow + n_\downarrow}, \tag{3.46}$$

where $n_\uparrow$ and $n_\downarrow$ are filling factors as defined above. For $P = 0$ this situation represents the classic BCS state. When $P \neq 0$, this is breached pair (BP) or Sarma phase. There is some debate in the literature [50, 51, 52] on whether BP is a stable phase. For a fixed chemical potential difference, the mean field gap equation (3.35) has a non-zero solution, but this solution corresponds to a maximum of the free energy and thus in this scheme BP is not a stable phase. However, when the densities and not the chemical potentials are fixed, the solution of the gap equation corresponds to a minimum of the free energy and thereby to a stable phase. Bedaque et al. pointed out that this solution might still be energetically unfavorable, when compared to a phase separation, see below [53]. As opposed to the calculations of Bedaque et al. our results show that in the lattice this model gives a stable BP phase in a large part of the phase diagram, see figure 3.1, even when the phase separation is taken into account. It was suggested by a recent quantum Monte Carlo study that in fact both the schemes described above will give the same physics [54].

In the BP phase, the leftover atoms in the majority component form an unpaired region or "breach" around the smaller Fermi surface, shown in figure 3.2. The transition between BCS and BP is continuous, i.e. there is no phase transition between these two. Indeed, BCS is the $P \to 0$ limit of BP. With higher polarizations, however, it is possible that the difference of chemical potentials

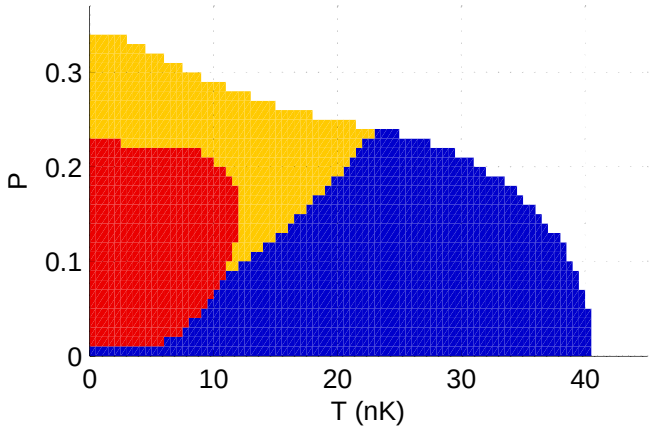

FIGURE 3.1: Temperature-polarization phase diagram for a Fermi gas in an optical lattice. The average filling fraction in this diagram is 0.2. The color coding of the different phases is: blue: BCS/BP, red: phase separation, yellow: FFLO, white: normal state. These results were published in publication III. The Hubbard parameters are $U = -0.26E_R$ and $J = 0.07E_R$. The values for temperatures correspond to ^{6}Li atoms in a lattice created by lasers with wavelength 1030 nm.

is so large that in fact the gap in the quasiparticle spectrum disappears. Such a state is often called a gapless superfluid. It is important to note that in the scheme where the filling factors are fixed, BP can be stable for an arbitrarily small polarization and only a part of the BP region is actually gapless. It should be noted that it is customary to talk about a polarized or density imbalanced gas when dealing with any polarization other than 0. A system with $n_\uparrow = n_\downarrow$ is unpolarized or balanced.

The phase with $\Delta > 0$ and $|\mathbf{q}| > 0$ is known as the Fulde-Ferrel-Larkin-Ovchinnikov phase. For pairing, the non-zero FFLO momentum $\mathbf{q}$ shifts the Fermi surfaces relative to each other, causing pairing between atoms with momenta $\mathbf{k}$ and $-\mathbf{k} + 2\mathbf{q}$. Compared to BP, this leaves an asymmetric breach in momentum space, schematically drawn in figure 3.3. This breach might not even encircle the smaller surface. The $\mathbf{q} \to 0$ limit of FFLO is BP, but there is a second order phase transition between these phases.

When either the temperature or polarization is too high, it is energetically favorable for the system to be in the normal non-superconducting phase, behaving like an ideal Fermi gas. The occupation number of a single particle state with energy $\xi_\mathbf{k}$ is given by $n_F(\xi_\mathbf{k})$.

It is also possible for a polarized system to minimize its free energy by separating into regions of unpolarized superfluid and polarized normal fluid. Such

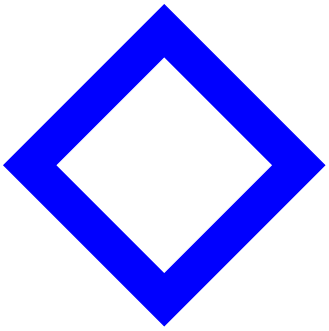

FIGURE 3.2: Unpaired region (breach) of majority atoms around the rectangular Fermi surface of minority atoms.

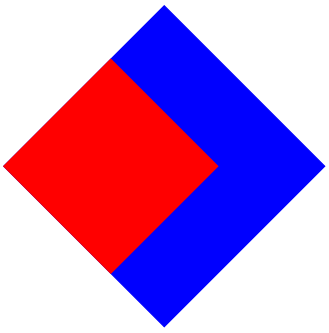

FIGURE 3.3: Asymmetric unpaired region of majority atoms.

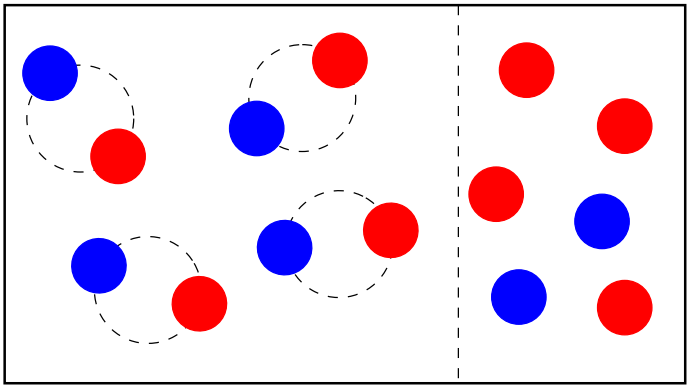

FIGURE 3.4: A schematic diagram of phase separation into an unpolarized BCS state and polarized normal state.

a setup is typically called phase separation and was first studied theoretically in the context of Fermi gases by Bedaque et al. [53]. The free energy analysis is the following: assume that there are $N_\uparrow$ atoms in the majority component and $N_\downarrow$ atoms in the minority component, in a lattice with M lattice sites. Assume also that the BCS phase occupies the fraction x of the total volume of the lattice and that there are N_{BCS} atoms from both species in the BCS phase. This means that there are $N_\uparrow - N_{BCS}$ majority component atoms and $N_\downarrow - N_{BCS}$ minority component atoms in the normal phase, occupying a total number of $(1-x)M$ lattice sites, see figure 3.4. The free energy of the system in total is therefore

$$\begin{aligned} F_{total} =& xF_{BCS}\left(n_\uparrow = \frac{N_{BCS}}{xM}, n_\downarrow = \frac{N_{BCS}}{xM}\right) \\ &+ (1-x)F_{normal}\left(n_\uparrow = \frac{N_\uparrow - N_{BCS}}{(1-x)M}, n_\downarrow = \frac{N_\downarrow - N_{BCS}}{(1-x)M}\right). \end{aligned} \tag{3.47}$$

There are actually two free variables in this scheme: x and N_{BCS}. It would seem natural that N_{BCS} always assumes its maximum value, $N_\downarrow$, putting all the minority atoms in the paired phase, but this does not minimize the free energy of the phase separated system. Some minority atoms are always unpaired. No boundary effects are incorporated into the theory, and therefore the results tell us nothing of the distribution of these phases in the volume.

3.5 Density effects and the van Hove singularity

For standard mean-field BCS-type superfluidity in the single band Hubbard model in 3D, the effect of density is quite simple: the gap attains its maximum

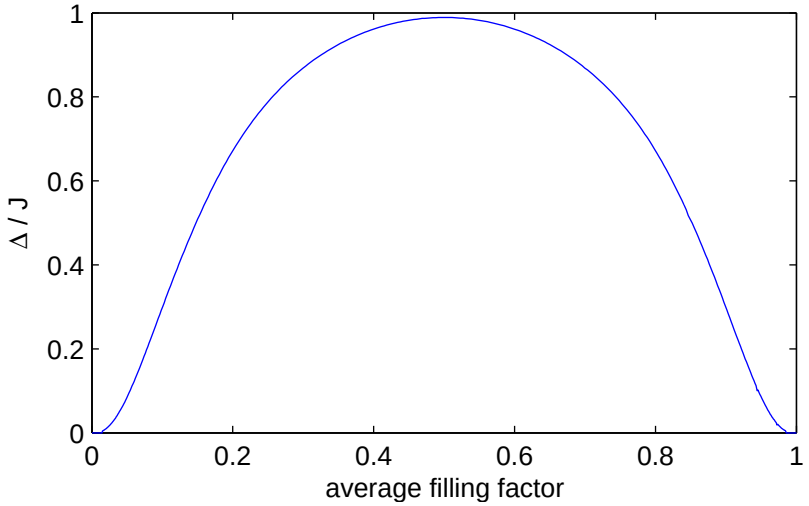

FIGURE 3.5: The BCS gap Δ as a function of the average filling fraction of atoms, in the units of hopping energy in a 3D lattice with $U/J \approx 3.7$. The gap is largest at half filling. The curve is symmetric due to the particle-hole symmetry.

value at half filling and goes to zero as the density approaches either zero or unity. This is because for densities below half filling, the BCS gap scales with the increasing Fermi energy, and, on the other hand, because of the particle-hole symmetry, the same limit should be arrived at while approaching half filling from above. Also, as the density per spin component approaches unity, tunnelling in the lowest band is suppressed because of Pauli blocking. In fact, with one fermion of each species in each lattice site, the system becomes a band insulator, where any tunnelling requires an excitation to a higher band. The BCS pairing gap is plotted in figure 3.5 as a function of density. It has been suggested that because this treatment neglects any interactions between the pairs, it exaggerates the pairing gap for high densities [55]. The pairing paradigm can also be approached from a different perspective by simply solving the two-body SchrÃ¶dinger equation and excluding the Pauli blocked modes from the wavefunction. This method gives a binding energy for the pairs that is maximized with filling factors below half filling [56].

Another remarkable feature of a lattice potential is the Van Hove singularity. The following derivation may help to understand the problem. Assuming a dispersion relation $\epsilon(\mathbf{k})$, the total number of states $N(E)$ below energy E is

given by

$$N(E) = \int_{\epsilon(\mathbf{k})\leqslant E} g_{\mathbf{k}}\, d\mathbf{k}, \tag{3.48}$$

where $g_{\mathbf{k}}$ is the density of states in momentum space. Because ϵ is a smooth function, the integral can be rewritten in terms of surfaces of constant energy E', integrated from 0 to E. Assuming the energy difference between two such surfaces is ΔE, their distance $s(\mathbf{k})$ at point $\mathbf{k}$ in the direction perpendicular to the inner surface, i.e. to the direction of $\nabla\epsilon$, follows to first order the following equation: $\Delta E = |\nabla\epsilon(\mathbf{k})|s(\mathbf{k})$. If the energy is split into M equally spaced intervals, each with the thickness $\Delta E = E/M$, their total volume $N_M(E)$ is

$$\sum_{n=0}^{M-1}\left(\int_{\epsilon(\mathbf{k})=n\Delta E} s(\mathbf{k})g_{\mathbf{k}}\, d\mathbf{k}\right) = \sum_{n=0}^{M-1}\left(\int_{\epsilon(\mathbf{k})=n\Delta E} \frac{\Delta E}{|\nabla\epsilon(\mathbf{k})|} g_{\mathbf{k}}\, d\mathbf{k}\right). \tag{3.49}$$

Now $N(E)$ can be written as

$$N(E) = \lim_{M\to\infty} N_M(E) = \int_0^E \left(\int_{\epsilon(\mathbf{k})=E'} \frac{g_{\mathbf{k}}}{|\nabla\epsilon|}\, d\mathbf{k}\right) dE' \tag{3.50}$$

and the density of states at energy E as

$$g(E) = \frac{dN(E)}{dE} = \int_{\epsilon(\mathbf{k})=E} \frac{g_{\mathbf{k}}}{|\nabla\epsilon|}\, d\mathbf{k}. \tag{3.51}$$

The Van Hove singularity means a point where $|\nabla\epsilon| = 0$, thus causing a divergence in the integrand in (3.51). Note that the surface of constant energy E has one dimension less than the momentum space. This means that in a one-dimensional problem there is no surface integral and therefore the divergence is directly in the density of states. In comparison, in a three-dimensional lattice the divergence is integrable, i.e. the integral converges and $g(E)$ itself is always finite, but it has a corner or a "kink" at the locations of Van Hove singularities.

In an ultracold Fermi gas in an optical lattice the Van Hove singularity causes interesting effects when the Fermi energy equals the energy of the singularity. Because the Fermi energy is determined by the filling fraction, and vice versa, this can be seen as a density effect. The dispersion relation in an n-dimensional cubic lattice is, assuming the hopping energy is J in all directions:

$$\epsilon(\mathbf{k}) = \sum_{i=1}^{n} 2J\,(1-\cos(k_i)) \tag{3.52}$$

and

$$|\nabla \epsilon| = \sqrt{\sum_{i=1}^{n} 4J^2 \sin^2(k_i)}. \tag{3.53}$$

In such a lattice, the singularity plays a prominent role when the density is just high enough for a point of the Fermi surface to reach the edge of the first Brillouin zone, i.e when the Fermi surface contains a point with one component of $\mathbf{k}$ equal to π and the rest equal to 0. At such a point $\epsilon(\mathbf{k}) = 4J$ regardless of dimensions, and because $\mu = \epsilon(\mathbf{k})$ for the points on the Fermi surface, $\mu = 4J$ when the singularity is reached. However, the shape of the Fermi surface with $\mu = 4J$ depends on the dimension. In 1D this is the chemical potential of a full lattice, which is a band insulator in the single band model. In 2D it corresponds to half filling while in 3D the filling factor is about 0.21 for one species.

In addition to the singularity, density affects the shape of the Fermi surface in all dimensions higher than one. With very small filling factors, i.e. when only the lowest part of the cosine dispersion is populated, the surface is almost spherical. When the density is increased, the shape of the surface becomes more like a square (in 2D) or octahedron (in 3D). These shapes are reached at $\mu = 4J$, as explained above. Beyond this, the shape bulges and finally fills up the first Brillouin zone. The shapes in the 2D case are shown in figure 3.6. In a strict sense, the concept of Fermi surface does not exist in an interacting system, but the interaction strengths used in this work are weak enough to only slightly distort the edge of the surface, making it fuzzy. Thus arguments related to Fermi surfaces can be used to qualitatively understand the behaviour of the system even in the interacting case. Of course, these arguments are valid only close to zero temperature, because higher temperatures smear the edges.

In a density imbalanced system, an effect can also be seen when the density of one of the components (usually the majority species) is at the Van Hove singularity. This effect presents itself as a change in the curvature of the FFLO-normal phase boundary, shown in figure 3.7. For example, in a 3D lattice, when the filling factors of the majority and minority species are on different sides of the singularity, the shapes of the Fermi surfaces are different, reducing the pairing gap. In the phase diagram, this is seen in the growth of the critical difference of the chemical potentials as a function of the average chemical potential: when μ_{aver} approaches half filling, $d\delta\mu_C/d\mu_{aver} > 0$, but the slope is much smaller in the region between the dashed lines, where $\mu_\uparrow > 4J$ but $\mu_\downarrow < 4J$. In 2D, this effect is so strong that between the points where $\mu_\uparrow = 4J$ and $\mu_\downarrow = 4J$, the critical chemical potential difference is reduced.

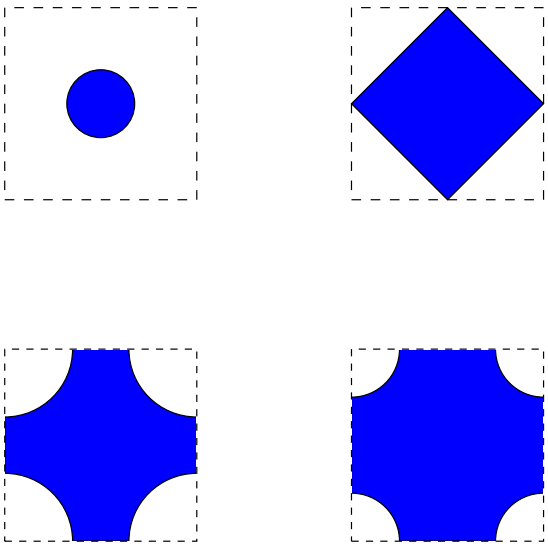

FIGURE 3.6: Fermi surfaces in a 2D cubic lattice, with increasing density.

3.6 Phase diagrams of a homogeneous system

Phase diagrams for a homogeneous system, i.e. one with constant filling factors $n_\uparrow$ and $n_\downarrow$ throughout the system, were calculated as follows: for each point of the phase diagram, the densities were calculated from polarization as $n_\uparrow = (1 + P/2)n$ and $n_\downarrow = (1 - P/2)n$, where n is the average density desired. Then the Helmholtz free energy (3.45) was minimized in each point, all the time making sure that the number equations (3.32) and (3.33) were satisfied. After the minimum free energy as a function of Δ and $\mathbf{q}$ was calculated in each point and thus the stable phase determined in accordance with the description of each phase given above, this free energy was compared with the free energy of a phase-separated state. One such diagram, with average filling fraction of 0.2, is shown in figure 3.1. Although this density is far from half filling and therefore does not produce the largest possible superfluid area, it shows a very "lattice-like" behaviour because of the proximity to the 3D Van Hove singularity.

The temperature-polarization phase diagram in figure 3.1 shows all the possible phases. In a density balanced system, with $P = 0$, the stable phase at zero temperature is BCS. The value of Δ at $T, P = 0$ is often denoted with Δ_0. The BCS critical temperature, i.e. the temperature at which the system undergoes a

phase transition between BCS and normal state is usually called T_C. The ratio of Δ_0/k_BT_C is a numerical constant that depends on the dispersion relation of the system; for a box potential this constant is approximately 1.764 [57]. The highest polarization that allows superfluidity is called critical polarization, P_C, and it depends on temperature. In this phase diagram P_C is 0.35, but with a higher interaction strength the mean field theory would allow critical polarizations as high as 1. At the time of writing there are no experimental results on the critical polarization in a 3D lattice.

Figure 3.8 shows a ground state phase diagram of a polarized Fermi gas in an optical lattice. The highest critical polarization for FFLO is above the average filling fraction of 0.2. This is due to the shapes of the Fermi surfaces: as explained above, at this density the 3D Fermi surface closely resembles an octahedron. The free energy advantage of FFLO compared to e.g. BP is that in the optimal FFLO configuration the magnitude of $\mathbf{q}$ is such that the Fermi surfaces of majority and minority atoms touch, and as two octahedra touch at one point so that one is within the other, they automatically touch on a larger area. Optimally their corners touch, leading to half the surface area of the smaller octahedron to touch the larger one. Not surprisingly, numerical analysis shows that the FFLO free energy is always lowest at such a configuration, i.e. $\mathbf{q}$ is along one of the axes. When either the temperature increases from zero or the average density per component is moved away from 0.21, this effect decreases. With similar arguments, the same effect is expected to appear in a 2D lattice at half filling.

It is possible to further expand this analysis with the same theory by allowing a phase separation into FFLO and normal state. Compared to the phase separation of BCS and normal state, this would add more complexity to the calculation, because $n_\uparrow$ need not equal $n_\downarrow$ in the FFLO phase. Because this would increase the computation time by more than a factor of 10, doing the calculation is beyond the scope of this study.

Phase diagrams allowing the possibility of FFLO and phase separation have been calculated for a Fermi gas in free space [58, 59]. FFLO appears in a smaller area of the phase diagrams in these systems than it does in the lattice. This is probably due to shapes of the Fermi surfaces, as explained above. It has been predicted that FFLO is stable also in a one-dimensional lattice [60, 61, 62].

3.7 Harmonic confinement

As explained above in the context of optical lattices, there is always a harmonic potential superimposed on the lattice. The simple homogeneous density mean

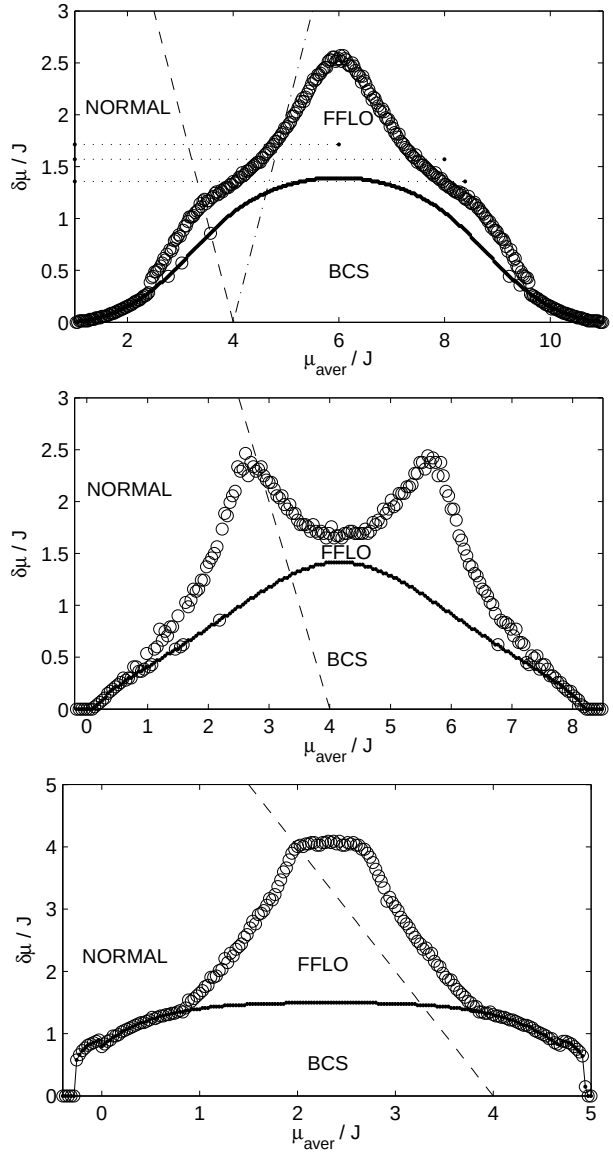

FIGURE 3.7: Phase diagrams with constant chemical potentials in 3D, 2D, and 1D lattices, from top to bottom, as functions of $\mu_{\text{aver}} = (\mu_\uparrow + \mu_\downarrow)/2$ and $\delta\mu = \mu_\uparrow - \mu_\downarrow$. The solid line is the critical value of $\delta\mu$ for BCS and the circles represent $\delta\mu_C$ for FFLO. The isolated circles falling on the solid line are convergence errors due to the numerical method. All the diagrams are at $T = 0$. The declining dashed lines show where $\mu_\uparrow = 4J$, i.e. the Van Hove singularity of the majority component. The inclining dashed line in the 3D diagram shows where $\mu_\downarrow = 4J$ and the horizontal dotted lines correspond to the shell structures in figure 3.9. The lower dimensional systems were simulated with a 3D lattice with reduced hopping strength(s) in the orthogonal direction(s). These results were originally published in publication IV.

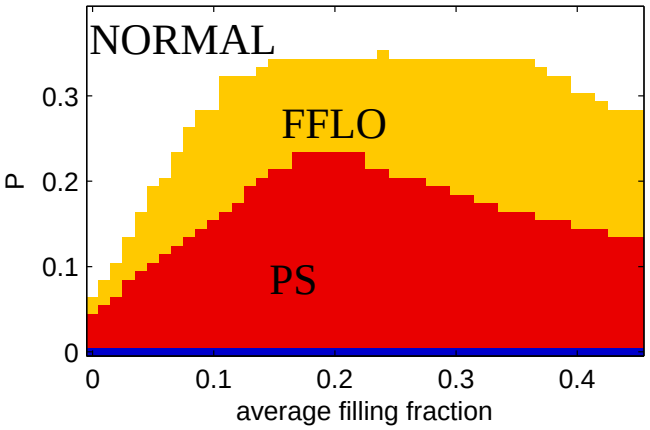

FIGURE 3.8: Ground state ($T = 0$) phase diagram for a Fermi gas in an optical lattice. This diagram displays data originally published in publication III. The calculation was done with the same parameters as in figure 3.1. Here the regions are: BCS on the $P = 0$ line (blue), phase separation (PS, red), FFLO with $|q| > 0$ (FFLO, yellow), and normal phase (NORMAL, white).

field theory presented above cannot take into account this additional potential, but the so called *local density approximation* (LDA) can. The idea is to define a new local chemical potential $\mu'(\mathbf{r})$ so that

$$\mu = \mu'(\mathbf{r}) + V(\mathbf{r}), \tag{3.54}$$

where $V(\mathbf{r})$ is the harmonic potential, is a constant. Because both the species experience the same harmonic confinement, the difference in chemical potentials is also a constant, independent of position. The scheme works in the following way: assign the values for the chemical potentials in the origin, $\mu_\uparrow$ and $\mu_\downarrow$, and divide the system in equal sized cells. In each cell, find the stable phase by minimizing the free energy with fixed chemical potentials $\mu'_\uparrow = \mu_\uparrow - V(\mathbf{r})$ and $\mu'_\downarrow = \mu_\downarrow - V(\mathbf{r})$ using the center of the cell as $\mathbf{r}$. These calculations are done as if the cell size was infinite. The number of particles in each cell is calculated directly from filling factors given the number equations (3.32) and (3.33), multiplied by the real cell size and the total numbers by summing up the cells. There are no boundary effects or correlations between the cells included in the description.

The fact that there can only be one fermion of any species in a lattice site produces very interesting shell structures. This is because in the lattice, the results depend qualitatively on the average density, as shown in figure 3.5. For example, if there are a lot of particles overall in the trap, the chemical potential

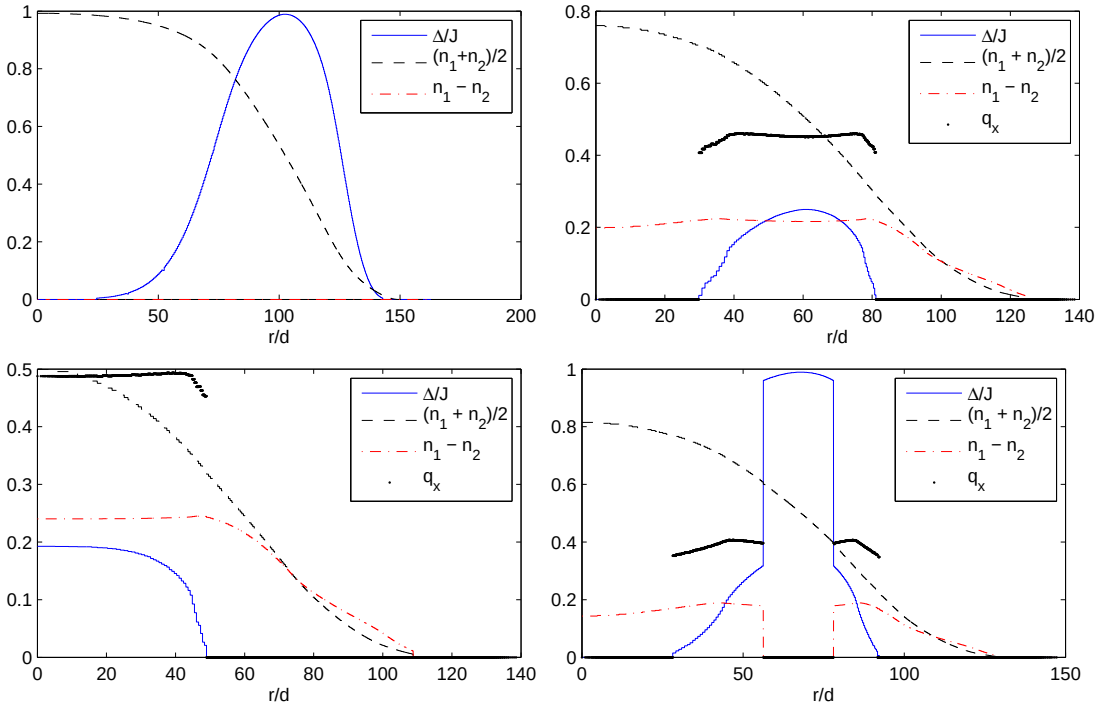

FIGURE 3.9: Shell structures for an ultracold gas in a 3D optical lattice, calculated with LDA. In each figure, the black dashed line shows the local average density, $(n_\uparrow + n_\downarrow)/2$, the red dash-dotted line the difference of densities, $n_\uparrow - n_\downarrow$, the blue solid line the pairing gap Δ in units of the hopping parameter, and the black dots the FFLO wavevector q. The differences in chemical potentials are (in units of the hopping parameter): top left, 0, top right, 1.6, bottom left, 1.7, and bottom right, 1.4.

in the center will be very high and the filling factors in the center are close to unity. This means that there is no superfluidity in the center but rather a core of normal gas. As the local density is reduced away from the center, the core is surrounded by shells of different phases, such as FFLO and BCS. Finally at the edge the gas is too dilute for superfluid phases and the outermost shell is in the normal phase. All such structures can be read directly from the phase diagrams in figure 3.7 as they correspond to horizontal lines in the diagrams. Typical shell structures are shown in figure 3.9.

FFLO-like order parameter oscillations have also been predicted for trapped systems without the lattice [63, 64, 65]. It has also been suggested that in a two-dimensional lattice in harmonic confinement, the order parameter would oscillate radially with low densities and axially with high densities [66].

3.8 Detection

Recognizing different phases is not as straightforward in a quantum gas as it is in a solid state system. Measuring temperature-conductivity curves of a metal wire is already well established, whereas measuring just the temperature of a dilute cloud is still a challenge. Therefore schemes for detecting the different phases have to be thought out carefully. Superfluidity in itself can be confirmed by observing quantized vortices [31], and the value of the pairing gap can be measured with radio frequency spectroscopy [28, 29]. Phase separation of a population imbalanced gas into regions of unpolarized and polarized gases can be detected for instance by imaging both species independently [67, 68] or by observing the difference of the density profiles by phase contrast imaging [69].

At the time of writing, the FFLO phase has not been observed unequivocally in any system, although there are some experiments [70, 71, 72, 73, 74, 75] in solid state systems that suggest the existence of this state. Even though some quantities are hard to measure, ultracold Fermi gases seem to be the best candidate for directly observing FFLO. Due to the form of the order parameter, FFLO has several unique signatures, such as differences in the momentum distributions of the two species, shown in publications II and III. Clear signals in the density noise correlations have also been predicted, as FFLO creates "empty" areas in momentum space where the signal drops to zero [76, 77]. The characteristic oscillations of the order parameter have also been suggested to be observable with radio frequency spectroscopy [78] and the superfluid density of the FFLO phase has been predicted to differ dramatically from that of the BCS phase [79], which could be used to differentiate between these phases.

Chapter 4

Response to density perturbations: dimensional effects and application as a sensor

4.1 Linear response

Many spectroscopic methods function by creating a perturbation in the system and measuring the response to that perturbation. The response to a perturbation that couples directly to the density of the system is known as *density response*. For weak perturbations, the theory of linear response is enough to describe the process. Formally the Hamiltonian operator in this situation is of the form

$$\widehat{H} = \widehat{H}_0 + \widehat{H}_{ext} = \widehat{H}_0 + \int \hat{n}(\mathbf{r})\phi_{ext}(\mathbf{r}, t)\, d\mathbf{r}, \tag{4.1}$$

where $\phi_{ext}(\mathbf{r}, t)$ is the external perturbation. The response to this perturbation is a change in density, formally given by

$$\delta\rho(\mathbf{r}, t) = \langle \hat{n}(\mathbf{r}, t)\rangle_{\widehat{H}} - \langle \hat{n}(\mathbf{r}, t)\rangle_{\widehat{H}_0}. \tag{4.2}$$

Taking into account only terms linear in ϕ, the following equation can be derived in frequency-momentum space [80]:

$$\delta\rho(\mathbf{q}, \omega) = \chi(\mathbf{q}, \omega)\phi_{ext}(\mathbf{q}, \omega). \tag{4.3}$$

Here $\chi(\mathbf{q}, \omega)$ is the susceptibility of the gas to perturbations of this kind. This means that to solve the problem completely, it is enough to solve χ. It should be noted that unlike in the previous chapter, $\mathbf{q}$ does not refer to the FFLO wavevector, it is simply the momentum. To calculate χ in a way that takes into account collective behaviour and not just quasiparticle excitations is not straightforward. The calculation is more involved than for example the derivations of the previous chapter and therefore beyond the scope of this thesis. For a derivation the reader is referred to [81], here I will only give a brief overview of the formalism.

The method used is the generalized random phase approximation that assumes the system to be in the BCS state. Therefore regarding the equations of the previous chapter, the FFLO wavevector is zero and the chemical potentials are equal, $\mu_\uparrow = \mu = \mu_\downarrow$. In order to derive an equation for χ, let us define the following matrices:

$$L^0(\mathbf{q},\omega) = \begin{pmatrix} L^0_{1111} & L^0_{1121} & L^0_{1211} & L^0_{1221} \\ L^0_{1112} & L^0_{1122} & L^0_{1212} & L^0_{1222} \\ L^0_{2111} & L^0_{2121} & L^0_{2211} & L^0_{2221} \\ L^0_{2112} & L^0_{2122} & L^0_{2212} & L^0_{2222} \end{pmatrix}, \tag{4.4}$$

$$\widetilde{A}(\mathbf{q}) = \begin{pmatrix} u_\mathbf{q}^2 & u_\mathbf{q} v_\mathbf{q} \\ -u_\mathbf{q} v_\mathbf{q} & -v_\mathbf{q}^2 \end{pmatrix}, \tag{4.5}$$

and

$$\widetilde{B}(\mathbf{q}) = \begin{pmatrix} v_\mathbf{q}^2 & -u_\mathbf{q} v_\mathbf{q} \\ u_\mathbf{q} v_\mathbf{q} & -u_\mathbf{q}^2 \end{pmatrix}. \tag{4.6}$$

With the components L^0_{ijkl} given by

$$\begin{aligned} L^0_{ijkl}(\mathbf{q},\omega) = \sum_{\mathbf{q}'} \Bigg(& \frac{\widetilde{A}_{ij}(\mathbf{q}+\mathbf{q}')\widetilde{A}_{kl}(\mathbf{q}')\,(n_F(E_\mathbf{q}) - n_F(E_{\mathbf{q}'} - E_\mathbf{q}))}{E_{\mathbf{q}'} - E_{\mathbf{q}+\mathbf{q}'} + \hbar(\omega + i\delta)} \\ & + \frac{\widetilde{B}_{ij}(\mathbf{q}+\mathbf{q}')\widetilde{B}_{kl}(\mathbf{q}')\,(n_F(E_\mathbf{q}) - n_F(E_{\mathbf{q}'} - E_\mathbf{q}))}{E_{\mathbf{q}'} - E_{\mathbf{q}+\mathbf{q}'} - \hbar(\omega + i\delta)} \\ & + \frac{\widetilde{A}_{ij}(\mathbf{q}+\mathbf{q}')\widetilde{B}_{kl}(\mathbf{q}')\,(n_F(E_\mathbf{q}) + n_F(E_{\mathbf{q}'} - E_\mathbf{q}) - 1)}{E_{\mathbf{q}'} + E_{\mathbf{q}+\mathbf{q}'} - \hbar(\omega + i\delta)} \\ & + \frac{\widetilde{B}_{ij}(\mathbf{q}+\mathbf{q}')\widetilde{A}_{kl}(\mathbf{q}')\,(n_F(E_\mathbf{q}) + n_F(E_{\mathbf{q}'} - E_\mathbf{q}) - 1)}{E_{\mathbf{q}'} + E_{\mathbf{q}+\mathbf{q}'} + \hbar(\omega + i\delta)} \Bigg). \end{aligned} \tag{4.7}$$

Here $i\delta$ is a convergence factor related to the complex integral. In a numerical calculation, δ has to have a non-zero value for the calculation to converge. This produces a finite line width, which is heuristically similar to that of an experiment. Although L^0 is a 4×4 matrix, it is shown in [81] that it only has six independent elements, denoted in the following way:

$$\begin{aligned} a &= L_{1111} = L_{2222} \\ b &= L_{1212} = -L_{1221} = -L_{2112} = L_{2121} \\ c &= L_{1112} = -L_{1121} = L_{1222} = -L_{2122} \\ \bar{c} &= L_{1211} = -L_{2111} = L_{2212} = -L_{2221} \\ d &= L_{1122} \\ \bar{d} &= L_{2211}. \end{aligned} \tag{4.8}$$

The susceptibility is given by

$$\chi(\mathbf{q}, \omega) = \frac{x_1 + x_4}{1 - U(x_1 + x_4)}, \tag{4.9}$$

where U is the interaction parameter and $\mathbf{x}$ is the solution of

$$\left(\mathbb{1} + UL^0\right)\mathbf{x} = \hat{L}, \tag{4.10}$$

where

$$\hat{L} = \begin{pmatrix} a - b \\ 2c \\ 2\bar{c} \\ a - b \end{pmatrix}. \tag{4.11}$$

The formalism in itself is independent of the single particle dispersion, which enters only in the quasiparticle energies E and Bogoliubov coefficients u and v.

4.2 Sound velocity and the Bogoliubov-Anderson phonon

A Fermi gas has two kinds of possible excitations in response to a perturbation: collective and single (quasi)particle. The collective excitation in a superfluid Fermi gas is known as the Bogoliubov-Anderson phonon and its dispersion is shown in figure 4.1. The phonon is not gapped, meaning that it can be excited with energy below 2Δ, which is the threshold for breaking the Cooper pairs. Close to $\mathbf{k} = 0$ the dispersion is linear, i.e. group velocity $d\omega/dk$ of the phonon is constant. This is the physical velocity of the phonon and it corresponds to the velocity of sound in the system. All the results are for a balanced mixture, with $n_\uparrow = n_\downarrow$.

In publication I we have calculated the dependence of the velocity of sound on several variables in an optical lattice. Perhaps the most interesting one is density, because of the Van Hove singularity. As a function of density, the speed of sound has a minimum at total filling fraction $n = 0.42$, as shown in figure 4.2. This is due to the fact that the density of states, and therefore compressibility, has a maximum at the location of the singularity. Qualitatively this can be understood in the following way: with more states of the same energy available to scatter to, the system is easier to compress, and therefore collective modes do not travel fast. Interactions weaken this effect because the edge of the Fermi surface is smeared.

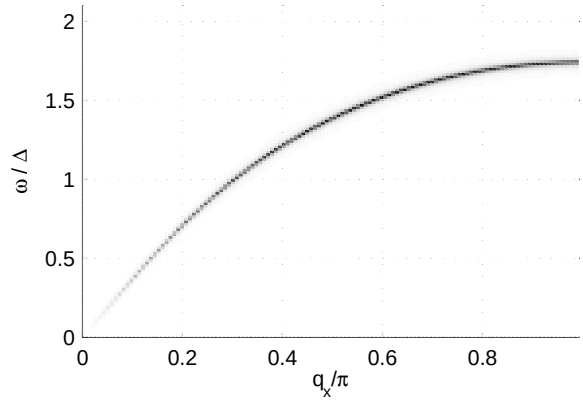

FIGURE 4.1: The dispersion of the Bogoliubov-Anderson phonon in a three-dimensional lattice, calculated from the location of the peak in $(\mathbf{q}, \omega)$ space. In the long-wavelength, small-q limit the dispersion is linear, but saturates towards the edge of the first Brillouin zone.

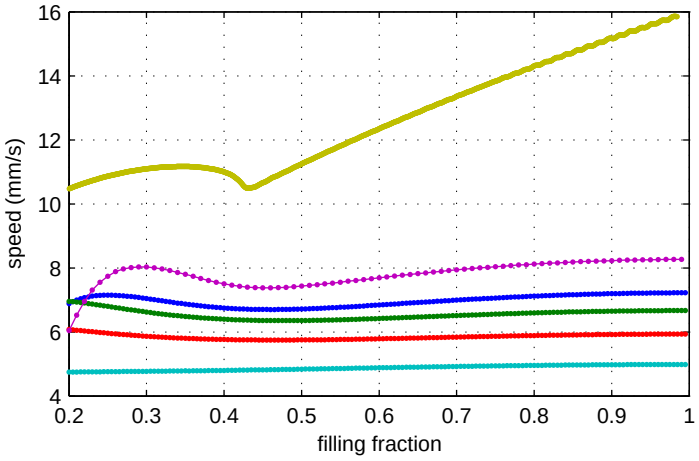

FIGURE 4.2: Speed of sound in a three-dimensional lattice as a function of total filling fraction, for different interaction strengths. The top curve corresponds to a non-interacting Fermi gas, and the lower ones to increasing interaction strength: 2.5, 3.3, 4.0, 5.0, and 6.6, from top to bottom, in the units of U/J. The minimum corresponds to the Van Hove singularity where $E_F = 4J$.

The dependence of the speed of sound on the filling fraction changes qualitatively with the effective dimensionality of the lattice. The cubic symmetry can be broken by adjusting the hopping strengths in different directions by changing the lattice heights: for a cubic lattice, $s_x = s_y = s_z$, whereas $s_x = s_y < s_z$ corresponds to a situation where the system consists of two-dimensional sheets, often called "pancakes", with suppressed tunnelling between them. On the other hand, with $s_x = s_y > s_z$, the lattice resembles a set of parallel tubes, where tunnelling along the tubes, i.e. in the z-direction, is stronger than in the orthogonal directions. The shape of the filling fraction - speed curve depends qualitatively on these ratios, as shown in figures 4.3 and 4.4. In the cubic symmetric case there is a local minimum at the location of the three-dimensional van Hove singularity, whereas in the case of pancakes, the location of the minimum shifts towards half filling, the location of the two-dimensional singularity. In the case of (effectively) one-dimensional tubes, the speed along the symmetry axis increases monotonously with the increasing filling fraction, which is qualitatively reasonable: with higher density the collective mode propagates faster.

4.3 Application as a sensor

Ultracold atomic Bose gases have been used in the detection of magnetic fields [82, 83] on atom chips [84, 85, 86]. The measurement works by trapping and cooling the gas in the vicinity of a chip with an electric circuit, and measuring the changes of the center-of-mass location of the cloud, caused by the magnetic field of the circuit. Such a setup offers a combination of sensitivity and resolution presently unavailable by other methods [83].

Applying a superfluid Fermi gas as a sensor allows an extra degree of tunability in the form of the pairing gap. Since the minimum energy needed to break a Cooper pair is 2Δ, the energy required to excite two quasiparticles just above the pairing gap, a perturbation with frequency below $2\Delta/\hbar$ can not create quasiparticles. This could be exploited in experiments in the following way: the value of Δ is adjusted with Feshbach resonance and gradually lowered. Each time $2\Delta/\hbar$ goes below a frequency present in the signal, the number of quasiparticles excited goes up sharply. The quasiparticles can be detected for example by radio-frequency spectroscopy [87, 88, 28, 89].

The idea is described on the following model: the perturbation consists of a superposition of modes with frequencies ω_i and therefore the magnetic field

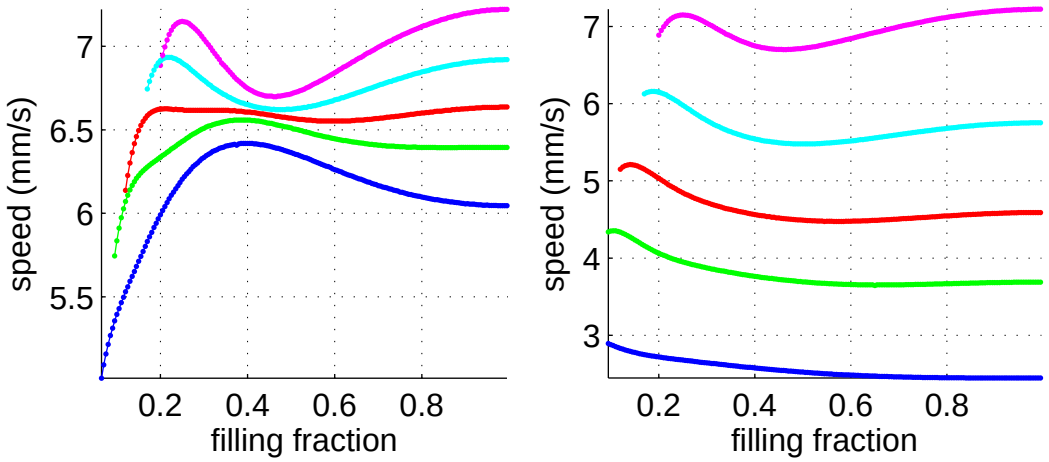

FIGURE 4.3: Speed of sound in a lattice with cubic symmetry broken by $s_x = s_y < s_z$. The figure on the left shows speed along x, i.e. in the plane parallel to the pancakes, and the one on the right the speed along the z-axis. The curves correspond to different ratios of s_x/s_z: (from top to bottom) 1.0, 0.83, 0.71, 0.62, and 0.5.

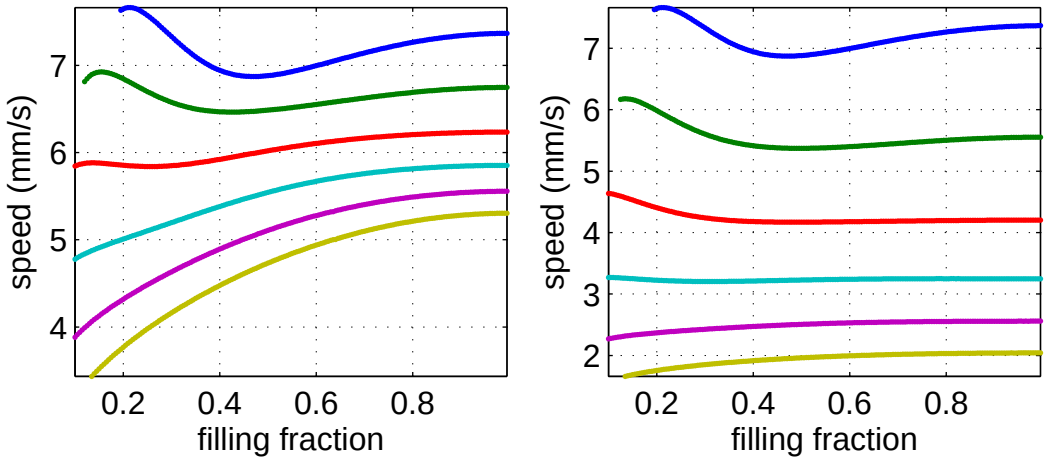

FIGURE 4.4: Speed of sound in a lattice with cubic symmetry broken by $s_x = s_y > s_z$. The figure on the left shows speed in the direction of the tubes, z, and the other one speed orthogonal to the tubes. The curves correspond to different ratios of s_x/s_z: (from top to bottom) 1.0, 1.2, 1.4, 1.6, 1.8, and 2.0.

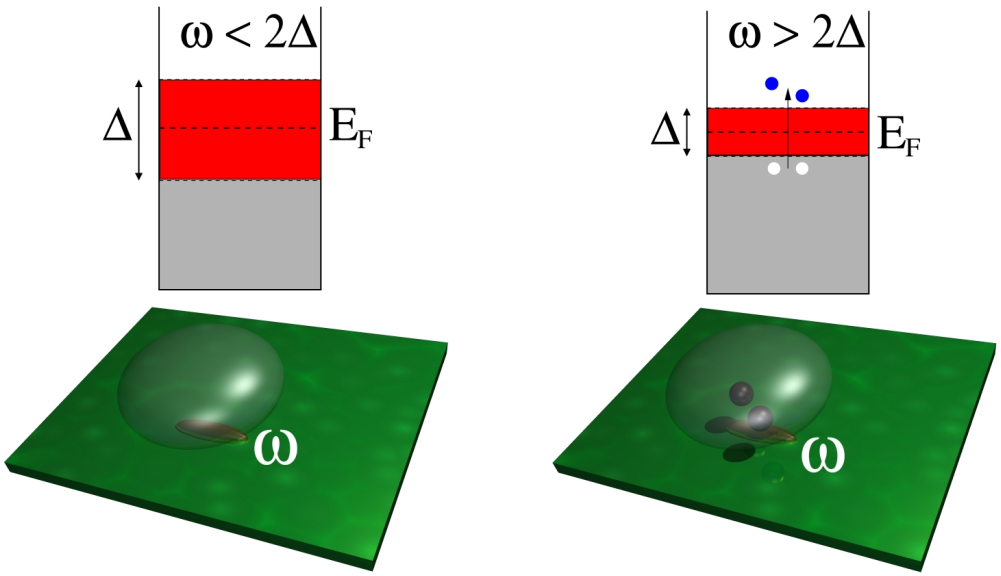

FIGURE 4.5: A schematic figure of the Fermi sensor. When the frequency of the magnetic field is below $2\Delta/\hbar$, quasiparticles are not excited. If Δ is lowered enough, the same frequency can create quasiparticles, which can be detected.

has the spectrum

$$\mathbf{B}(\omega, \mathbf{q}) = \sum_i \mathbf{A}_i \delta(\omega - \omega_i)\varphi_i(\mathbf{q}). \tag{4.12}$$

The wavevector dependence $\varphi(\mathbf{q})$ is due to the geometry of the perturbation and it is independent of frequency, which ensures that $\varphi_i(\mathbf{q})$ is the same for all modes, i.e. $\varphi_i(\mathbf{q}) = \varphi(\mathbf{q})$. Since neutral atoms in hyperfine state m_F experience the magnetic field as a potential of strength

$$V = g\mu_B m_F B, \tag{4.13}$$

where $\mu_B = e\hbar/2m$ is the Bohr magneton and $g \approx 2$ is the Landé factor, this field creates density perturbations in the gas. These perturbations are of the form

$$\delta\rho(\mathbf{q}, \omega) = \chi(\mathbf{q}, \omega)\varphi(\mathbf{q}) \sum_i A_i \delta(\omega - \omega_i). \tag{4.14}$$

To understand the behaviour of this system as a sensor it is enough to study the dynamical structure factor $S(\mathbf{q}, \omega)$:

$$S(\mathbf{q}, \omega) = -\frac{1}{\pi} \mathrm{Im}\chi(\mathbf{q}, \omega). \tag{4.15}$$

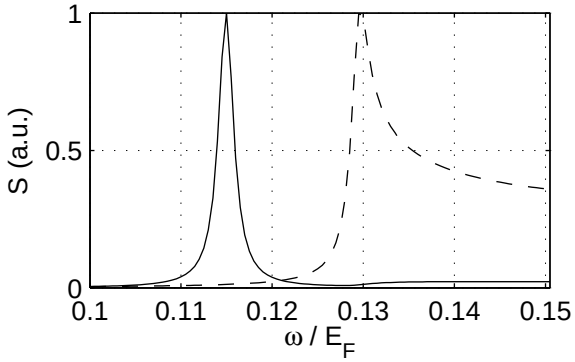

FIGURE 4.6: The dynamic structure $S(\mathbf{q}, \omega)$ as a function of frequency ω for two values of momentum, $q = 0.2k_F$ and $q = 0.4k_F$. Here $2\Delta \approx 0.13E_F$. The amplitude of the phonon peak is much larger than that of the quasiparticle continuum for the smaller momentum. With the larger momentum the frequency of the phonon is very close to the pairing gap and the peak connects with the continuum.

Because the present micro traps do not contain an optical lattice, all the calculations presented herein are done for a system with the single particle dispersion $\epsilon(\mathbf{k}) = \hbar^2 k^2/2m$. The results are presented in Fermi units, where the unit of energy is the Fermi energy E_F and the unit of momentum is the Fermi wavevector $k_F = \sqrt{2mE_F/\hbar^2}$. Also S is given in arbitrary units.

Because it may be possible the observe the quasiparticles independently of the phonon, for example with radiofrequency spectroscopy, we present some of the results in two forms: the full signal, and the same signal with frequencies below $2\Delta/\hbar$ removed. This is particularly effective with small q, since for low momenta the phonon peak is separate from the quasiparticle continuum and has very high amplitude, as shown in figure 4.6.

The results of a scan of values of Δ between 0 and 0.1 are shown in figure 4.7. The perturbation signal is the sum of four frequencies, $S = A_1 S(\mathbf{q}, \omega_1) + A_2 S(\mathbf{q}, \omega_2) + A_3 S(\mathbf{q}, \omega_3) + A_4 S(\mathbf{q}, \omega_4)$, plotted as a function of the pairing gap Δ, with all the amplitudes A_i equal to one.

In publication V we have also shown that the detection of the spin of single electron should be feasible with this method, provided that the gas can be trapped within 500 nm of the chip.

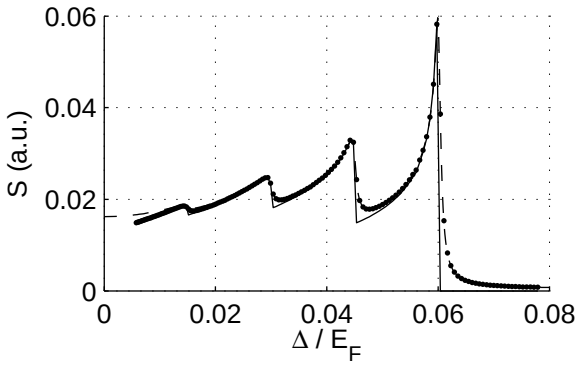

FIGURE 4.7: Dynamic structure factor as a function of pairing gap Δ, summed for frequencies 0.03, 0.06, 0.09, and 0.12 (in the units of $E_F/\hbar$). The dots show the full calculation and the solid line the results with the signal suppressed for $\hbar\omega < 2\Delta$. Here $q = 0.4k_F$.

Chapter 5

Conclusions

The mean field theory presented in this thesis is one of the first steps towards understanding the behaviour of a spin population imbalanced ultracold Fermi gas in a three-dimensional optical lattice. The results show that the Fulde-Ferrel-Larkin-Ovchinnikov state benefits energetically from the shape of the Fermi surface in a square lattice and thus FFLO fills a large area in the corresponding phase diagram. It has also been shown that the local density approximation predicts very interesting shell structures to appear when the lattice is combined with a harmonic trap. Thus FFLO is likely to be easier to observe in an optical lattice than with just a harmonic trap.

In the second part I have studied some dynamical properties of ultracold Fermi gases, both with and without an optical lattice. The results show how a dimensional crossover between effectively one-, two-, and three-dimensional lattices is reflected in the speed of sound. The last publication included in the thesis suggests a qualitatively new detection method for magnetic and electric fields, utilizing the pairing gap of superfluid Fermi gas.

There are at least three directions in which the theory for ultracold Fermi gases in optical lattices could be expanded. One is the inclusion of correlation effects beyond mean field, another is connecting these correlations with a finite temperature and the third is a more careful treatment of the underlying harmonic potential. Although theoretical methods exist already for doing some of these in a one-dimensional lattice, implementing them for three-dimensional lattices remains a challenge for the future.

Bibliography

[1] S. N. BOSE. *Plancks gesetz und lichtquantenhypothese*. Z. Phys. **26**, 178 (1924).

[2] A. EINSTEIN. *Quantentheorie des einatomigen idealen Gases: Zweite Abhandlung*. Sitzungber. Preuss. Akad. Wiss. **1925**, 3 (1925).

[3] M. H. ANDERSON, J. R. ENSHER, M. R. MATTHEWS, C. E. WIEMAN, AND E. A. CORNELL. *Observation of Bose-Einstein condensation in a dilute atomic vapor*. Science **269**, 198 (1995).

[4] K. B. DAVIS, M.-O. MEWES, M. R. ANDREWS, N. J. VAN DRUTEN, D. S. DURFEE, D. M. KURN, AND W. KETTERLE. *Bose-Einstein condensation in a gas of sodium atoms*. Phys. Rev. Lett. **75**, 3969 (1995).

[5] C. J. PETHICK AND H. SMITH. *Bose-Einstein Condensation in Dilute Gases*. CUP, Cambridge (2001).

[6] U. FANO. *Effects of configuration interaction on intensities and phase shifts*. Phys. Rev. **124**, 1866 (1961).

[7] H. FESHBACH. *A unified theory of nuclear reactions*. Ann. Phys **19**, 287 (1962).

[8] S. INOUYE, M. R. ANDREWS, J. STENGER, H. J. MIESNER, D. M. STAMPER-KURN, AND W. KETTERLE. *Observation of Feshbach resonances in a Bose-Einstein condensate*. Nature **392**, 151 (1998).

[9] M. BARTENSTEIN, A. ALTMEYER, S. RIEDL, R. GEURSEN, S. JOCHIM, C. CHIN, J. H. DENSCHLAG, R. GRIMM, A. SIMONI, E. TIESINGA, C. J. WILLIAMS, AND P. S. JULIENNE. *Precise determination of ^{6}Li cold collision parameters by radio-frequency spectroscopy on weakly bound molecules*. Phys. Rev. Lett. **94**, 103201 (2005).

[10] J. BARDEEN, L. N. COOPER, AND J. R. SCHRIEFFER. *Theory of superconductivity*. Phys. Rev. **108**, 1175 (1957).

[11] D. EAGLES. *Possible pairing without superconductivity at low carrier concentrations in bulk and thin-film superconducting semiconductors*. Phys. Rev. **186**, 456 (1969).

[12] A. LEGGETT. *Diatomic molecules and cooper pairs*. In *Proceedings of*

the XVI Karpacz winter school of theoretical physics, page 13. Springer-Verlag, Berlin (1980).

[13] P. NOZIERES AND S. SCHMITT-RINK. *Bose condensation in an attractive fermion gas: From weak to strong coupling superconductivity*. J. Low Temp. Phys. **59**, 195 (1985).

[14] J. BEDNORZ AND K. MÜLLER. *Possible high T_C superconductivity in the Ba-La-Cu-O system*. Z. Physik, B **64**, 189 (1986).

[15] M. K. WU, J. R. ASHBURN, C. J. TORNG, P. H. HOR, R. L. MENG, L. GAO, Z. J. HUANG, Y. Q. WANG, AND C. W. CHU. *Superconductivity at 93 K in a new mixed-phase Y-Ba-Cu-O compound system at ambient pressure*. Phys. Rev. Lett. **58**, 908 (1987).

[16] C. A. REGAL, C. TICKNOR, J. L. BOHN, AND D. S. JIN. *Creation of ultracold molecules from a Fermi gas of atoms*. Nature **424**, 47 (2003).

[17] K. STRECKER, G. PARTRIDGE, AND R. HULET. *Conversion of an atomic Fermi gas to a long-lived molecular Bose gas*. Phys. Rev. Lett. **91**, 080406 (2003).

[18] J. CUBIZOLLES, T. BOURDEL, S. J. J. M. F. KOKKELMANS, G. V. SHLYAPNIKOV, AND C. SALOMON. *Production of long-lived ultracold Li molecules from a Fermi gas*. Phys. Rev. Lett. **91**, 240401 (2003).

[19] S. JOCHIM, M. BARTENSTEIN, A. ALTMEYER, G. HENDL, C. CHIN, J. H. DENSCHLAG, , AND R. GRIMM. *Pure gas of optically trapped molecules created from fermionic atoms*. Phys. Rev. Lett. **91**, 240402 (2003).

[20] S. JOCHIM, M. BARTENSTEIN, A. ALTMEYER, G. HENDL, S. RIEDL, C. CHIN, J. H. DENSCHLAG, AND R. GRIMM. *Bose-Einstein condensation of molecules*. Science **302**, 2101 (2003).

[21] C. REGAL, M. GREINER, AND D. JIN. *Emergence of a molecular Bose-Einstein condensate from a Fermi gas*. Nature **426**, 537 (2003).

[22] M. W. ZWIERLEIN, C. A. STAN, C. H. SCHUNCK, S. M. F. RAUPACH, S. GUPTA, Z. HADZIBABIC, AND W. KETTERLE. *Observation of Bose-Einstein condensation of molecules*. Phys. Rev. Lett. **91**, 250401 (2003).

[23] T. BOURDEL, L. KHAYKOVICH, J. CUBIZOLLES, J. ZHANG, F. CHEVY, M. TEICHMANN, L. TARRUELL, S. J. J. M. F. KOKKELMANS, AND C. SALOMON. *Experimental study of the BEC-BCS crossover region in lithium 6*. Phys. Rev. Lett. **93**, 050401 (2004).

[24] C. REGAL, M. GREINER, AND D. JIN. *Observation of resonance condensation of fermionic atom pairs*. Phys. Rev. Lett. **92**, 040403 (2004).

[25] M. W. ZWIERLEIN, C. A. STAN, C. H. SCHUNCK, S. RAUPACH, A. KERMAN, AND W. KETTERLE. *Condensation of pairs of fermionic atoms near a Feshbach resonance*. Phys. Rev. Lett. **92**, 120403 (2004).

[26] J. KINAST, S. L. HEMMER, M. E. GEHM, A. TURLAPOV, AND J. E.

THOMAS. *Evidence for superfluidity in a resonantly interacting Fermi gas*. Phys. Rev. Lett. **92**, 150402 (2004).

[27] M. BARTENSTEIN, A. ALTMEYER, S. RIEDL, S. JOCHIM, C. CHIN, J. H. DENSCHLAG, AND R. GRIMM. *Crossover from a molecular Bose-Einstein condensate to a degenerate Fermi gas*. Phys. Rev. Lett. **92**, 120401 (2004).

[28] C. CHIN, M. BARTENSTEIN, A. ALTMEYER, S. RIEDL, S. JOCHIM, J. H. DENSCHLAG, AND R. GRIMM. *Observation of the pairing gap in a strongly interacting Fermi gas*. Science **305**, 1128 (2004).

[29] J. KINNUNEN, M. RODRIGUEZ, AND P. TÖRMÄ. *Pairing gap and in-gap excitations in trapped fermionic superfluids*. Science **305**, 1131 (2004).

[30] J. KINAST, A. TURLAPOV, J. E. THOMAS, Q. CHEN, J. STAJIC, AND K. LEVIN. *Heat capacity of a strongly interacting Fermi gas*. Science **307**, 1296 (2005).

[31] M. W. ZWIERLEIN, J. ABO-SHAEER, A. SCHIROTZEK, C. SCHUNCK, AND W. KETTERLE. *Vortices and superfluidity in a strongly interacting Fermi gas*. Nature **435**, 1047 (2005).

[32] J. D. JACKSON. *Classical Electrodynamics*. John Wiley & Sons, Hoboken, 3rd edition (1999).

[33] I. BLOCH, J. DALIBARD, AND W. ZWERGER. *Many-body physics with ultracold gases*. Rev. Mod. Phys. **80**, 885 (2008).

[34] J. K. CHIN, D. E. MILLER, Y. LIU, C. STAN, W. SETIAWAN, C. SANNER, K. XU, AND W. KETTERLE. *Evidence for superfluidity of ultracold fermions in an optical lattice*. Nature **443**, 961 (2006).

[35] N. W. ASHCROFT AND N. D. MERMIN. *Solid state physics*. Saunders College Publishing, New York (1976).

[36] M. KÖHL, H. MORITZ, T. STÖFERLE, K. GÜNTER, AND T. ESSLINGER. *Fermionic atoms in a three dimensional optical lattice: Observing Fermi surfaces, dynamics, and interactions*. Phys. Rev. Lett. **94**, 080403 (2005).

[37] T. STÖFERLE, H. MORITZ, K. GÜNTER, M. KÖHL, AND T. ESSLINGER. *Molecules of fermionic atoms in an optical lattice*. Phys. Rev. Lett. **96**, 030401 (2006).

[38] N. STROHMAIER, Y. TAKASU, K. GÜNTER, R. JÖRDENS, M. KÖHL, H. MORITZ, AND T. ESSLINGER. *Interaction-controlled transport of an ultracold Fermi gas*. Phys. Rev. Lett. **99**, 220601 (2007).

[39] R. MICNAS, J. RANNINGER, AND S. ROBASZKIEWICZ. *Superconductivity in narrow-band systems with local nonretarded attractive interactions*. Rev. Mod. Phys. **62**, 113 (1990).

[40] R. JÖRDENS, N. STROHMAIER, K. GÜNTER, H. MORITZ, AND T. ESSLINGER. *A Mott insulator of fermionic atoms in an optical lattice*. Nature **455**, 204 (2008).

[41] T. ROM, T. BEST, D. VAN OOSTEN, U. SCHNEIDER, S. FOELLING, B. PAREDES, AND I. BLOCH. *Free fermion antibunching in a degenerate atomic Fermi gas released from an optical lattice*. Nature **444**, 733 (2006).

[42] U. SCHNEIDER, L. HACKERMULLER, S. WILL, T. BEST, I. BLOCH, T. A. COSTI, R. W. HELMES, D. RASCH, AND A. ROSCH. *Metallic and insulating phases of repulsively interacting fermions in a 3d optical lattice* (2008). arXiv:0809.1464.

[43] K. HUANG AND C. N. YANG. *Quantum-mechanical many-body problem with hard-sphere interaction*. Phys. Rev. **105**, 767 (1957).

[44] D. JAKSCH, C. BRUDER, J. CIRAC, C. W. GARDINER, AND P. ZOLLER. *Cold bosonic atoms in optical lattices*. Phys. Rev. Lett. **81**, 3108 (1998).

[45] S. TSUCHIYA AND A. GRIFFIN. *Landau damping of Bogoliubov excitations in optical lattices at finite temperature*. Phys. Rev. A **72**, 053621 (2005).

[46] F. MARSIGLIO. *Evaluation of the BCS approximation for the attractive Hubbard model in one dimension*. Phys. Rev. B **55**, 575 (1997).

[47] P. FULDE AND R. A. FERRELL. *Superconductivity in a strong spin-exchange field*. Phys. Rev. **135**, A550 (1964).

[48] A. I. LARKIN AND Y. N. OVCHINNIKOV. *Nonuniform state of superconductors*. Zh. Eksp. Teor. Fiz. **47**, 1136 (1964).

[49] A. I. LARKIN AND Y. N. OVCHINNIKOV. *Nonuniform state of superconductors*. Sov. Phys. JETP **20**, 762 (1965).

[50] E. GUBANKOVA, E. MISHCHENKO, AND F. WILCZEK. *Breached superfluidity via p-wave coupling*. Phys. Rev. Lett. **94**, 110402 (2005).

[51] M. M. FORBES, E. GUBANKOVA, W. V. LIU, AND F. WILCZEK. *Stability criteria for breach pair superfluidity*. Phys. Rev. Lett. **94**, 017001 (2005).

[52] L. HE AND P. ZHUANG. *Stable Sarma state in two-band Fermi systems* (2008). arXiv:0805.4699.

[53] P. F. BEDAQUE, H. CALDAS, AND G. RUPAK. *Phase separation in asymmetrical fermion superfluids*. Phys. Rev. Lett. **91**, 247002 (2003).

[54] G. G. BATROUNI, M. J. WOLAK, F. HEBERT, AND V. G. ROUSSEAU. *Pair formation and collapse in imbalanced fermion populations with unequal masses* (2008). arXiv:0809.4549.

[55] C.-C. CHIEN, Q. CHEN, AND K. LEVIN. *Fermions with attractive interactions on optical lattices and what they imply for correlated systems* (2008). arXiv:0808.1900.

[56] J. P. MARTIKAINEN. *Cooper problem in a lattice*. Phys. Rev. A **78**, 035602 (2008).

[57] M. TINKHAM. *Introduction to Superconductivity*. Dover Publications, Inc., Mineola (2004).

[58] D. E. SHEEHY AND L. RADZIHOVSKY. *BEC-BCS crossover in magnetized Feshbach-resonantly paired superfluids*. Phys. Rev. Lett. **96**, 060401 (2006).

[59] L. HE, M. JIN, AND P. ZHUANG. *Loff pairing vs. breached pairing in asymmetric fermion superfluids*. Phys. Rev. B **73**, 214527 (2006).

[60] A. E. FEIGUIN AND F. HEIDRICH-MEISNER. *Pairing states of a polarized Fermi gas trapped in a one-dimensional optical lattice*. Phys. Rev. B **76**, 220508 (2007).

[61] M. M. PARISH, S. K. BAUR, E. J. MUELLER, AND D. A. HUSE. *Quasi-one-dimensional polarized Fermi superfluids*. Phys. Rev. Lett. **99**, 250403 (2007).

[62] M. RIZZI, M. POLINI, M. A. CAZALILLA, M. R. BAKHTIARI, M. P. TOSI, AND R. FAZIO. *Fulde-Ferrell-Larkin-Ovchinnikov superfluidity in one-dimensional optical lattices*. Phys. Rev. B **77**, 245105 (2008).

[63] K. MACHIDA, T. MIZUSHIMA, AND M. ICHIOKA. *Generic phase diagram of fermion superfluids with population imbalance*. Phys. Rev. Lett. **97**, 120407 (2006).

[64] J. KINNUNEN, L. M. JENSEN, AND P. TÖRMÄ. *Strongly interacting Fermi gases with density imbalance*. Phys. Rev. Lett. **96**, 110403 (2006).

[65] L. M. JENSEN, J. KINNUNEN, AND P. TÖRMÄ. *Non-BCS superfluidity in trapped ultracold Fermi gases*. Phys. Rev. A **76**, 033620 (2007).

[66] Y. CHEN, Z. D. WANG, F. C. ZHANG, AND C. S. TING. *Exploring exotic superfluidity of polarized ultracold fermions in optical lattices* (2007). arXiv:0710.5484.

[67] M. W. ZWIERLEIN, A. SCHIROTZEK, C. H. SCHUNCK, AND W. KETTERLE. *Fermionic superfluidity with imbalanced spin populations*. Science **311**, 492 (2006).

[68] G. B. PARTRIDGE, W. LI, R. I. KAMAR, Y. LIAO, AND R. G. HULET. *Pairing and phase separation in a polarized Fermi gas*. Science **311**, 506 (2006).

[69] Y. SHIN, M. W. ZWIERLEIN, C. H. SCHUNCK, A. SCHIROTZEK, AND W. KETTERLE. *Observation of phase separation in a strongly-interacting imbalanced Fermi gas*. Phys. Rev. Lett. **97**, 030401 (2006).

[70] H. A. RADOVAN, N. A. FORTUNE, T. P. MURPHY, S. T. HANNAHS, E. C. PALM, S. W. TOZER, AND D. HALL. *Magnetic enhancement of superconductivity from electron spin domains*. Nature **425**, 51 (2003).

[71] A. BIANCHI, R. MOVSHOVICH, C. CAPAN, P. G. PAGLIUSO, AND J. L. SARRAO. *Possible Fulde-Ferrell-Larkin-Ovchinnikov superconducting state in CeCoIn5*. Phys. Rev. Lett. **91**, 187004 (2003).

[72] K. KAKUYANAGI, M. SAITO, K. KUMAGAI, S. TAKASHINA, M. NOHARA, H. TAKAGI, AND Y. MATSUDA. *Texture in the superconducting order*

parameter of CeCoIn5 revealed by nuclear magnetic resonance. Phys. Rev. Lett. **94**, 047602 (2005).

[73] V. F. MITROVIĆ, M. HORVATIĆ, C. BERTHIER, G. KNEBEL, G. LAPERTOT, AND J. FLOUQUET. *Observation of spin susceptibility enhancement in the possible Fulde-Ferrell-Larkin-Ovchinnikov state of $CeCoIn_5$*. Phys. Rev. Lett. **97**, 117002 (2006).

[74] V. F. CORREA, T. P. MURPHY, C. MARTIN, K. M. PURCELL, E. C. PALM, G. M. SCHMIEDESHOFF, J. C. COOLEY, AND S. W. TOZER. *Magnetic field induced lattice anomaly inside the superconducting state of CeCoIn5: evidence of the proposed Fulde-Ferrell-Larkin-Ovchinnikov state*. Phys. Rev. Lett. **98**, 087001 (2007).

[75] S. YONEZAWA, S. KUSABA, Y. MAENO, P. AUBAN-SENZIER, C. PASQUIER, AND D. JEROME. *Magnetic-field variations of the pair-breaking effects of superconductivity in (TMTSF)2ClO4*. J. Phys. Soc. Jpn. **77**, 054712 (2008).

[76] A. LUSCHER, R. M. NOACK, AND A. LAEUCHLI. *The FFLO state in the one-dimensional attractive Hubbard model and its fingerprint in the spatial noise correlations*. Phys. Rev. A **78**, 013637 (2008).

[77] T. PAANANEN, T. K. KOPONEN, P. TÖRMÄ, AND J.-P. MARTIKAINEN. *Density-density correlations of the ultra-cold Fermi gas in an optical lattice*. Phys. Rev. A **77**, 053602 (2008).

[78] M. BAKHTIARI, M. LESKINEN, AND P. TÖRMÄ. *Spectral signatures of the FFLO order parameter in one-dimensional optical lattices*. Phys. Rev. Lett. **101**, 120404 (2008).

[79] T. PAANANEN. *Superfluid-density of the ultra-cold Fermi gas in optical lattices* (2008). `arXiv:0811.3623`.

[80] M. PLISCHKE AND B. BERGERSEN. *Equilibrium statistical physics*. World Scientific, Hackensack, 3rd edition (2006).

[81] R. CÔTÉ AND A. GRIFFIN. *Cooper-pair-condensate fluctuations and plasmons in layered superconductors*. Phys. Rev. B **48**, 10404 (1993).

[82] S. WILDERMUTH, S. HOFFERBERTH, I. LESANOVSKY, E. HALLER, L. ANDERSSON, S. GROTH, I. BAR-JOSEPH, P. KRÜGER, AND J. SCHMIEDMAYER. *Microscopic magnetic-field imaging*. Nature **435**, 440 (2005).

[83] S. WILDERMUTH, S. HOFFERBERTH, I. LESANOVSKY, S. GROTH, P. KRÜGER, AND J. SCHMIEDMAYER. *Sensing electric and magnetic fields with Bose-Einstein condensates*. Appl. Phys. Lett. **88**, 264103 (2006).

[84] R. FOLMAN, P. KRÜGER, D. CASSETTARI, B. HESSMO, T. MAIER, AND J. SCHMIEDMAYER. *Controlling cold atoms using nanofabricated surfaces: atom chips*. Phys. Rev. Lett. **84**, 4749 (2000).

[85] R. FOLMAN, P. KRÜGER, J. SCHMIEDMAYER, J. DENSCHLAG, AND

C. HENKEL. *Microscopic atom optics: from wires to an atom chip*. Adv. At. Mol. Opt. Phys. **48**, 263 (2002).

[86] J. FORTÁGH AND C. ZIMMERMANN. *Magnetic microtraps for ultracold atoms*. Rev. Mod. Phys. **79**, 235 (2007).

[87] C. REGAL AND D. JIN. *Measurement of positive and negative scattering lengths in a Fermi gas of atoms*. Phys. Rev. Lett. **90**, 230404 (2003).

[88] S. GUPTA, Z. HADZIBABIC, M.W.ZWIERLEIN, C. STAN, K. DIECKMANN, C. SCHUNCK, E. VAN KEMPEN, B. VERHAAR, AND W. KETTERLE. *Radio-frequency spectroscopy of ultracold fermions*. Science **300**, 1723 (2003).

[89] J. KINNUNEN, M. RODRIGUEZ, AND P. TÖRMÄ. *Signatures of superfluidity for Feshbach-resonant Fermi gases*. Phys. Rev. Lett. **92**, 230403 (2004).